

1I/‘OUMUAMUA AND THE PROBLEM OF SURVIVAL OF OORT CLOUD COMETS NEAR THE SUN

ZDENEK SEKANINA

Jet Propulsion Laboratory, California Institute of Technology, 4800 Oak Grove Drive, Pasadena, CA 91109, U.S.A.

Version May 8, 2019

ABSTRACT

A 2000–2017 set of long-period comets with high-quality orbits of perihelion distance <1 AU is used to show that the objects that perish shortly before perihelion are nearly exclusively the Oort Cloud members, especially those with perihelia within 0.6 AU of the Sun, intrinsically fainter, and dust poor. Their propensity for disintegration is much higher than predicted by Bortle’s perihelion survival rule, prompting the author to propose a new synoptic index to be tested in future prognostication efforts. By their susceptibility to demise near the Sun, the nuclei of Oort Cloud comets differ dramatically from the nuclei of other long-period comets that almost always survive. In this scenario, ‘Oumuamua — discovered after perihelion — is in all probability a major piece of debris of an interstellar comet that was bound to perish near perihelion if it was similar to, though much fainter than, the known Oort Cloud comets. The nondetection of ‘Oumuamua by the Spitzer Space Telescope is compatible with optical data for pancake shape, but not for cigar shape, with the maximum dimension not exceeding 160 m (at an 0.1 albedo). Although the solar radiation pressure induced nongravitational acceleration requires very high porosity, ‘Oumuamua’s estimated mass is orders of magnitude greater than for a cloud of unbound submicron-sized dust grains of equal cross section. The acceleration could have displaced ‘Oumuamua by 250 000 km in 50 days, scattering other potential debris over a large volume of space.

Subject headings: comets: individual (1I/‘Oumuamua, C/1801 N1, X/1872 X1, C/1925 X1, C/1961 O1, C/1989 Q1, C/1989 X1, C/1991 X2, C/1991 Y1, C/1993 Q1, C/1996 N1, C/1999 S4, C/2000 S5, C/2000 W1, C/2000 WN₁, C/2001 A2, C/2001 Q4, C/2002 F1, C/2002 O4, C/2002 O6, C/2002 O7, C/2002 T7, C/2002 V1, C/2002 X5, C/2002 Y1, C/2003 T4, C/2004 F4, C/2004 H6, C/2004 R2, C/2004 S1, C/2004 V13, C/2005 A1, C/2005 K2, C/2006 A1, C/2006 M4, C/2006 P1, C/2006 WD₄, C/2007 F1, C/2007 T1, C/2007 W1, C/2008 J4, C/2009 O2, C/2009 R1, C/2010 F4, C/2010 X1, C/2011 C1, C/2011 L4, C/2011 M1, C/2012 C2, C/2012 F6, C/2012 S1, C/2012 T5, C/2013 G5, C/2013 K1, C/2013 R1, C/2013 US₁₀, C/2013 V5, C/2014 C2, C/2014 E2, C/2014 Q1, C/2015 C2, C/2015 F3, C/2015 G2, C/2015 P3, C/2016 R3, C/2016 U1, C/2016 VZ₁₈, C/2017 E1, C/2017 E4, C/2017 S3, C/2017 T1, C/2017 T3, 2P, 3D, 5D, 20D, 96P) — methods: data analysis

1. INTRODUCTION

My suggestion that 1I/‘Oumuamua’s parent body had failed to reach perihelion intact (Sekanina 2019) was based on the presumed affinity between its physical behavior and the behavior of intrinsically faint, dynamically new comets arriving from the Oort Cloud. The argument further employed the results of a paper on the **perihelion survival limit** by Bortle (1991), who noticed that virtually no fainter comets with perihelion distances less than 0.25 AU have ever been observed after perihelion, because they perished. Bortle also determined the perihelion-distance dependent limiting absolute magnitude H_{surv} (normalized to unit distances from the Sun and Earth) that a comet has to have in order to survive perihelion passage. He approximated the observed absolute magnitude with Vsekhsvyatsky’s (1958) quantity H_{10} , which assumes that the visual brightness varies inversely as a fourth power of heliocentric distance.

Bortle’s set of comets with perihelion distance smaller than 0.5 AU, observed between 1800 and 1988 and fainter than the survival limit H_{surv} , consisted of 23 objects, divided into three groups. The most extensive was the

no-survival group with 16 members, while the *survival* group (i.e., objects contradicting the rule) contained a single object. The intermediate, *unstable-survival* group was made up of the remaining six comets. This group appears to be rather heterogeneous; it includes C/1925 X1 (old designation 1926 III, Ensor), which was observed as a headless tail, the product of preperihelion debris, on the only four post-perihelion exposures available (Sekanina 1984), having obviously perished near perihelion. The group also includes C/1961 O1 (old designation 1961 V, Wilson-Hubbard), which was still centrally condensed on the plates exposed by Tomita (1962) nearly four months after perihelion — clearly a survivor.

For some, especially the early 19th-century comets on Bortle’s (1991) list, it is uncertain whether they were missed after perihelion because of their sudden fading or because nobody was searching for them, given that no ephemeris was available. For example, for comet C/1801 N1, the first entry on Bortle’s list, Kronk (2003) lists no report on efforts aimed at recovering the object after perihelion.

One of the 16 nonsurvivors on the list, X/1872 X1, was an inadvertent product of a search for 3D/Biela and its existence was so questionable and orbit so uncertain

(Kronk 2003) that it is not even listed in the Marsden & Williams (2008) *Catalogue of Cometary Orbits*. There surely is no evidence whatsoever on its post-perihelion evolution.

Yet, the most severe problem with the data that Bortle could do nothing about was the inferior quality of the orbital elements for nearly all comets in his set. For fully 20 of the 23 comets, or 87 percent, only parabolic elements were available. This explains why Bortle said his results applied to *long-period* comets, a very broad category. It included members of the Kreutz sungrazing system on the one hand and Oort Cloud comets on the other, thus encompassing a range of orbital periods exceeding four orders of magnitude, from less than 1000 years to more than 10 million years.

The inferior quality of the orbital elements was the corollary of the poor quality of astrometry in early times and of short orbital arcs observed for nearly all comets on Bortle’s list, which in turn were in part the product of the early, preperihelion termination of the observations due to the overly diffuse appearance of the objects.

Nearly thirty years after Bortle’s (1991) pioneering work it is time to revisit the problem of perihelion survival, to test his conclusions on a set of high-quality orbital data, with the aim of avoiding the pitfalls that he could not circumvent. Of particular importance is to find out whether all faint long-period comets with small perihelion distance have the tendency to perish or whether this propensity is typical for a certain group or groups. Because of the presumed affinity of ‘Oumuamua to Oort Cloud comets, they are the primary focus of this study.

2. LONG-PERIOD COMETS WITH SMALL PERIHELION DISTANCES DISCOVERED IN 2000–2017

In the era of the Sky Survey Projects, of which the most recent and successful example is PanSTARRS, comets are often discovered at considerably larger heliocentric distances than ever before. With the parallel substantial progress in the imaging and image-reduction techniques, the orbital elements for early discovered comets, including their orbital periods, are determined in most cases with very high accuracy.

To begin with, I employed the on-line comet catalog by S. Yoshida¹ to select, from the list of all comets discovered between 2000 and 2017, those with a perihelion distance of less than 1 AU, an orbital period greater than 1000 years, and an observed orbital arc of more than 10 days. The choices for the orbital period and orbital arc, which may look extreme, are justified as they secure a broad range of initial conditions. The orbital-period limit excludes the Kreutz sungrazers, including C/2011 W3, from the set.

The resulting set includes 60 comets, presented in Table 1. The individual columns list, respectively, the designation; the perihelion time, t_π (in TT); the perihelion distance, q (in AU); the original barycentric reciprocal semimajor axis (measuring the orbital period), $(1/a)_{\text{orig}}$, and its mean error (in AU^{-1}); the observed orbital arc, Δt_{obs} , the temporal distance of the first, t_{beg} , and the last, t_{last} , astrometric observations from the time of perihelion, $\Delta t_{\text{beg}} = t_{\text{beg}} - t_\pi$ and $\Delta t_{\text{last}} = t_{\text{last}} - t_\pi$ (all in days); the observed (preperihelion) absolute magni-

tude, H_0 ; the absolute magnitude at Bortle’s limit of perihelion survival, H_{surv} ; and the reference to the source of the original semimajor axis.

The elements t_π , q , and $(1/a)_{\text{orig}}$ were extracted from the circulars (NK) issued by S. Nakano,² primarily because he lists the residuals from individual astrometric observations that provide information on the quality of the orbital solution. For several remaining comets the elements were taken from the *Minor Planet Center’s* website³ (MPC) or from specific comprehensive investigations mentioned below. The information on the observed orbital arc was taken from the MPC; t_{beg} and t_{last} are the times of the actual first and last astrometric observations, respectively, regardless of whether they were used in the orbit determination. Time t_{beg} may precede the time of discovery, if precovery images were subsequently found and measured, or it may (slightly) lag behind the discovery time in a case of visual discovery. The observed absolute magnitude was extracted from the on-line catalog of photometric parameters by A. Kammerer,⁴ while the survival limit was derived from Bortle’s (1991) formula.

Inspection of Table 1 shows the presence of 20 Oort Cloud comets (33 percent of the total), whose orbital periods are nominally longer than 3 million years; a small group of 5 comets (8 percent) with the orbital periods of 150 000–1 000 000 years; 23 comets (38 percent) with the orbital periods of 2000–50 000 years; and 12 comets (20 percent) with the parabolic or poorly determined elliptic orbits, similar in quality to most entries in Bortle’s (1991) set; these will be all but ignored in the following.

3. SIGNS OF DISINTEGRATION OF A COMET NEAR PERIHELION

The issue now is which of the 60 comets survived perihelion and which perished. The decision is a difficult task that requires examination of the physical behavior of each object to test for the signs of disintegration. The symptoms and manifestations are as follows:

(1) Termination of astrometric observations. If a comet stops suddenly to be observed for position, this may be an indication that it lost the nuclear condensation and could no longer be measured. However, ground-based astrometry is also terminated when the comet gets too close to the Sun in the sky; if this is the case, the astrometric observations should resume after perihelion as soon as the elongation recovers. It is thus essential that for comets suspected of perishing near the Sun the elongation variations be examined during the critical period of time. To some extent, this problem is mitigated — but by no means eliminated — by the imaging capabilities of the solar space observatories, SOHO and STEREO.

(2) Display of progressively increasing, systematic residuals left by astrometric observations — in a period of time shortly before perihelion — from an orbital solution that fully satisfied the observations made only days earlier. This development is likely to mark the incipient phase of disintegration of the nucleus into a cloud of fragments and is typically accompanied by changes in the comet’s appearance.

² See <http://www.oaa.gr.jp/~oaacs/nk.htm>.

³ See https://minorplanetcenter.net/db_search.

⁴ See <http://fg-kometen.vdsastro.de/oldause.htm>.

¹ See <http://www.aerith.net/comet/catalog/index-code.html>.

Table 1

List of Comets Discovered in 2000–2017 Whose Perihelion Distances Are Less Than 1 AU and Orbital Periods Exceed 1000 Years

Comet ^a	Time of Perihelion, t_π (TT)	Perihelion Distance, q (AU)	Reciprocal Semimajor Axis ^b , $(1/a)_{\text{orig}}$ (AU^{-1})	Orbital Arc Observed ^c (d)			Abs. Magn., ^d H_0	Surv. Limit, ^e H_{Surv}	Reference
				Δt_{obs}	Δt_{beg}	Δt_{last}			
C/2000 S5	2000 Oct 26.7	0.605	0.0	45.8	-37.1	+8.7	9.8	8.5	NK 1516
C/2000 W1	2000 Dec 26.6	0.321	0.0	89.5	-30.2	+59.3	10.2	8.9	NK 817
C/2000 WM ₁	2002 Jan 22.7	0.555	+0.000522 ± 0.000001	981.9	-463.6	+518.3	7.5	10.3	NK 955
C/2001 A2	2001 May 24.5	0.779	+0.001113 ± 0.000003	319.0	-141.5	+177.5	7.5	11.7	NK 809B ^f
C/2001 Q4 [*]	2004 May 16.0	0.962	+0.000028 ± 0.000001	1820.3	-995.6	+824.7	5.6	12.8	NK 1037 ^g
C/2002 F1	2002 Apr 22.9	0.438	(+0.001048)	53.3	-33.7	+19.6	9.8	9.6	MPC ^h
C/2002 O4 [*]	2002 Oct 02.0	0.776	-0.000789 ± 0.000021	66.2	-66.4	-0.2	11	11.7	NK 979 ⁱ
C/2002 O6	2002 Sept 09.4	0.495	(+0.002782)	30.1	-38.7	-8.6	9.7	10.0	NK 981
C/2002 O7 [*]	2003 Sept 22.6	0.903	+0.000044 ± 0.000002	343.7	-420.4	-76.7	10.1	12.4	NK 982
C/2002 T7 [*]	2004 Apr 23.1	0.615	+0.000010 ± 0.000001	1255.4	-558.7	+696.7	4.9	10.7	NK 1038 ^j
C/2002 V1	2003 Feb 18.3	0.099	+0.002292 ± 0.000007	350.1	-103.7	+246.4	7.0	7.6	NK 1078 ^k
C/2002 X5	2003 Jan 29.0	0.190	+0.000893 ± 0.000011	128.5	-45.1	+83.4	7.2	8.1	NK 988 ^k
C/2002 Y1	2003 Apr 13.2	0.714	+0.004103 ± 0.000001	391.1	-105.8	+285.3	6.7	11.3	NK 967
C/2003 T4	2005 Apr 03.6	0.850	+0.000212 ± 0.000009	894.1	-538.2	+355.9	7.8	12.1	NK 1084
C/2004 F4	2004 Apr 17.1	0.168	+0.005133 ± 0.000013	154.2	-1.2	+153.0	8.3	8.0	NK 1121
C/2004 H6 [*]	2004 May 12.7	0.776	-0.000242 ± 0.000023	107.2	+3.7	+110.9	7.4	11.7	NK 1157
C/2004 R2	2004 Oct 07.9	0.113	0.0	18.0	-28.5	-10.5	10	7.7	NK 1240
C/2004 S1	2004 Dec 09.1	0.679	(+0.008734)	26.6	-73.8	-47.2	~20(?)	11.1	NK 1242 ^h
C/2004 V13	2004 Dec 21.2	0.181	0.0	13.0	+4.8	+17.8	7.2	8.1	NK 1248
C/2005 A1	2005 Apr 10.2	0.907	+0.000099 ± 0.000002	190.6	-121.7	+68.9	8.2	12.4	NK 1221 ^{k,l}
C/2005 K2 [*]	2005 Jul 05.4	0.545	-0.001554 ± 0.000160	33.5	-47.0	-13.5	13.5	10.3	NK 1378 ^l
C/2006 A1	2006 Feb 22.2	0.555	+0.000775 ± 0.000002	341.8	-48.2	+293.6	8.5	10.3	NK 1366
C/2006 M4	2006 Sept 28.7	0.783	+0.000194 ± 0.000002	433.2	-78.3	+354.9	6.5	11.7	NK 1641
C/2006 P1 [*]	2007 Jan 12.8	0.171	+0.000018 ± 0.000002	309.0	-158.3	+150.7	6.2	8.0	NK 1714
C/2006 WD ₄	2007 Apr 28.4	0.591	+0.002245 ± 0.000002	204.2	-159.1	+45.1	16(?)	10.5	NK 1476
C/2007 F1	2007 Oct 28.8	0.402	+0.000830 ± 0.000022	267.1	-251.5	+15.6	9.1	9.4	NK 1538
C/2007 T1	2007 Dec 12.5	0.969	+0.000611 ± 0.000003	183.9	-64.1	+119.8	7.7	12.8	NK 1727
C/2007 W1 [*]	2008 Jun 24.9	0.850	-0.000052 ± 0.000025	393.2	-217.4	+175.8	8.6	12.1	NK 1577 ^m
C/2008 J4	2008 Jun 19.5	0.448	0.0	14.9	-39.7	-24.8	16	9.7	MPC
C/2009 O2	2010 Mar 24.4	0.695	+0.000327 ± 0.000004	252.5	-240.1	+12.4	11.0	11.2	NK 1892R
C/2009 R1 [*]	2010 Jul 02.7	0.405	+0.000011 ± 0.000005	344.2	-347.0	-2.8	6.7	9.4	NK 1937
C/2010 F4	2010 Apr 06.1	0.614	0.0	12.0	-10.3	+1.7	14	10.7	MPC
C/2010 X1 [*]	2011 Sept 10.7	0.483	+0.000022 ± 0.000002	272.3	-275.6	-3.3	8.6	9.9	NK 2114
C/2011 C1	2011 Apr 18.0	0.883	+0.002846 ± 0.000002	308.4	-93.5	+214.9	9.4	12.3	NK 2181
C/2011 L4 [*]	2013 Mar 10.2	0.302	+0.000021 ± 0.0000002	1194.5	-658.8	+535.7	5.4	8.8	NK 2934 ⁿ
C/2011 M1 [*]	2011 Sept 07.6	0.896	-0.001770 ± 0.000547	41.0	-77.2	-36.2	9.5	12.4	NK 2428
C/2012 C2	2012 Mar 12.7	0.801	0.0	16.7	-30.6	-13.9	12.0	11.8	NK 2278
C/2012 F6	2013 Mar 24.5	0.731	+0.002182 ± 0.0000002	1009.4	-427.0	+582.4	5.2	11.4	NK 2939
C/2012 S1 [*]	2013 Nov 28.7	0.013	+0.000035 ± 0.000006	784.3	-790.1	-5.8	8.7	7.1	S+K'14 ^p
C/2012 T5 [*]	2013 Feb 24.1	0.323	-0.000202 ± 0.000018	157.8	-132.7	+25.1	11.0	8.9	NK 2420
C/2013 G5	2013 Sept 01.1	0.928	0.0	56.7	-140.6	-83.9	~20(?)	12.6	MPC
C/2013 K1	2013 May 30.0	0.949	0.0	50.3	-11.5	+38.8	18	12.7	MPC
C/2013 R1	2013 Dec 22.7	0.812	+0.002722 ± 0.000001	371.7	-106.0	+265.7	7.1	11.9	NK 2763
C/2013 US ₁₀ [*]	2015 Nov 15.7	0.824	+0.000023 ± 0.0000001	1576.2	-823.2	+753.0	4.9	11.9	NK 3482
C/2013 V5 [*]	2014 Sept 28.2	0.625	-0.000004 ± 0.000001	523.9	-320.1	+203.8	8.6	10.8	NK 2953
C/2014 C2	2014 Feb 18.2	0.512	+0.002371 ± 0.000020	80.0	-18.0	+62.0	16(?)	11.3	MPC
C/2014 E2	2014 Jul 02.5	0.664	+0.001230 ± 0.000001	452.9	-111.4	+341.5	6.8	11.0	NK 2960
C/2014 Q1	2015 Jul 06.5	0.315	+0.001182 ± 0.000002	636.2	-324.0	+312.2	7.9	8.9	NK 3304
C/2015 C2	2015 Mar 04.6	0.711	+0.001937 ± 0.000013	144.6	-7.2	+137.4	~12(?)	11.3	NK 2980
C/2015 F3	2015 Mar 09.3	0.834	+0.004546 ± 0.000041	67.1	+14.8	+81.9	~16(?)	12.0	MPC ^q
C/2015 G2 [*]	2015 May 23.8	0.780	+0.000023 ± 0.000002	314.0	-54.7	+259.3	8.4	11.7	NK 3054
C/2015 P3	2015 Jul 27.8	0.715	+0.005621 ± 0.000066	54.0	+12.6	+66.6	14(?)	11.3	MPC
C/2016 R3	2016 Oct 11.0	0.447	+0.005693 ± 0.001431	13.0	-29.9	-16.9	18(?)	9.7	MPC
C/2016 U1 [*]	2017 Jan 14.0	0.319	-0.000029 ± 0.000036	83.6	-84.7	-1.1	11.3	8.9	NK 3339 ^r
C/2016 VZ ₁₈	2017 Mar 07.4	0.910	+0.005084 ± 0.000003	289.8	-149.9	+139.9	18	12.5	NK 3340
C/2017 E1	2017 Apr 10.1	0.901	+0.000883 ± 0.000023	116.7	-40.0	+76.7	10.5	12.4	NK 3516
C/2017 E4 [*]	2017 Apr 23.3	0.494	-0.002482 ± 0.000122	46.1	-44.6	+1.5	11.7	10.0	MPC
C/2017 S3 [*]	2018 Aug 16.0	0.209	+0.000020 ± 0.000003	350.8	-363.7	-12.9	10.7	8.3	S+K'18 ^s
C/2017 T1	2018 Feb 21.7	0.581	+0.000205 ± 0.000013	261.6	-146.1	+115.5	12.3	10.5	NK 3527
C/2017 T3	2018 Jul 19.1	0.825	+0.001016 ± 0.000029	360.4	-310.5	+49.9	9.0	12.0	NK 3685

Notes to Table 1.

- ^a Oort Cloud comets are marked with a star.
^b Referred to the barycenter of the Solar System.
^c Columns give, respectively, total period covered by astrometric observations and times of first and last observations reckoned from time of perihelion.
^d Total absolute visual magnitude before perihelion (observed or extrapolated).
^e Absolute magnitude at survival limit, given by Bortle’s formula.
^f Nongravitational solution. Comet experienced several outbursts and split repeatedly; B was primary nucleus. Comet’s evolution was investigated in detail by Sekanina et al. (2002) and by Jehin et al. (2002).
^g Gravitational solution; nongravitational solutions are on NK 1126, NK 1265, and NK 1439.
^h Parenthesized $1/a$ is osculating value; no original orbit available.
ⁱ Orbital variations and related physical changes were investigated by Sekanina (2002); see Section 4 for details.
^j Gravitational solution; nongravitational solution is on NK 1438.
^k Nongravitational solution.
^l Comet split.
^m Gravitational solution; nongravitational solution for preperihelion arc of orbit is on NK 1731A.
ⁿ Orbit determined by T. Kobayashi.
^p Orbit from comprehensive investigation by Sekanina & Kracht (2014).
^q Member of group with C/1988 A1 (Liller) and C/1996 Q1 (Tabur); for details see Sekanina & Kracht (2016).
^r Oort Cloud membership somewhat uncertain.
^s Orbit from comprehensive investigation by Sekanina & Kracht (2018).

(3) Reports of one or more outbursts in the weeks before perihelion, followed by a sudden loss of nuclear condensation and subsequent disappearance of the object.

(4) Presence of a dust tail with a peculiar orientation and one boundary fairly sharp, indicating a sudden dramatic decline in the production of dust.

(5) Post-perihelion imaging observations at or close to the predicted location of the comet revealing an object whose appearance differs dramatically from that of the comet before perihelion, such as a headless tail, a diffuse and increasingly elongated cloud of debris, etc.

(6) A steep rate of the post-perihelion fading, resulting in major asymmetry relative to perihelion and accompanied by a drop in the degree of condensation (DC) in reports by visual observers.

(7) Reports of unsuccessful attempts to detect the comet visually or with a CCD sensor in an appropriate brightness range, contrary to expectation based on the preperihelion observations.

The rate at which the disintegration progresses varies from comet to comet and, if it is relatively slow, a limited number of post-perihelion observations is not ruled out. The ultimate issue of the nature and morphology of the nucleus’ debris is a largely unexplored territory to be addressed in Section 8.

Conservatively, each of the seven warning signs needs to be taken into consideration before deciding whether a comet survived or perished. Careful approach is particularly recommended for the Oort Cloud comets, which are notorious for post-perihelion fading at a rate that is always much steeper than preperihelion brightening (e.g., Whipple 1978); the greatly disappointing post-perihelion performance of the would-be “comet of the century” C/1973 E1 (Kohoutek), an Oort Cloud object, will never fade from the witnesses’ memory, even though technically the comet did not perish.

Generally, comets — from the Oort Cloud or otherwise — do not always behave consistently under the circumstances. If an object cannot be positively classified because of inconclusive evidence, only a conditional judgment is to be made or, in equivocal cases, none at all.

4. OORT CLOUD COMETS

For most of the 20 Oort Cloud comets in Table 1 the determination of the original orbit was straightforward. In particular, for both C/2012 S1 (ISON) and C/2017 S3 (PanSTARRS) the tabulated values were taken from orbital solutions by Sekanina & Kracht (2014, 2018), optimized for the purpose of obtaining a reliable original orbit. The result for C/2001 Q4 was taken from Nakano’s gravitational solution based on a shorter arc, rather than from the subsequent nongravitational solutions based on longer arcs (NK 1126, NK 1265, and NK 1439), given the potential problems with extracting an accurate original value once the nongravitational terms are incorporated into the equations of motion (Marsden et al. 1973). Similarly, Nakano’s gravitational orbits for C/2002 T7 and C/2007 W1 were preferred to his nongravitational orbits on, respectively, NK 1438 and NK 1731A. It is a matter of coincidence that for all three comets the introduction of the nongravitational acceleration turned out to have at most only a minor effect on the original orbit; there is no doubt about their having arrived from the Oort Cloud.

While it is well known that the nongravitational forces affect strongly the orbits of comets with small perihelion distances (Marsden et al. 1973, 1978), it was surprising to find that fully nine of the 20 Oort Cloud comets had the nominal original orbit hyperbolic. For three of them — C/2007 W1 (Boattini), C/2013 V5 (Oukaimeden), and C/2016 U1 (NEOWISE)— the hyperbolic excess was small, but for C/2004 H6 (SWAN), C/2005 K2 (LINEAR), C/2012 T5 (Bressi), and C/2017 E4 (Lovejoy) — for the last one the distribution of residuals being unavailable — it was in a range of $10\text{--}20\sigma$. For C/2005 K2, C/2011 M1 (LINEAR), and C/2017 E4 the hyperbolic excess is understood as part of the orbital uncertainties, as these comets were observed for fewer than 50 days. That still leaves two objects, C/2004 H6 and C/2012 T5, with $(1/a)_{\text{orig}}$ equaling $-0.000242 \pm 0.000023 \text{ (AU)}^{-1}$ and $-0.000202 \pm 0.000018 \text{ AU}^{-1}$, respectively, as the least likely cases of observational errors, given the satisfactory distributions of residuals. Based on 266 and 603 observations covering the orbital arcs of 107 and 158 days and leaving the mean residuals of $\pm 0''.69$ and $\pm 0''.82$, respectively, the two comets have a hyperbolic excess equivalent to a systematic velocity of nearly 0.5 km s^{-1} relative to the Sun at infinity.

Comet C/2004 H6 is exceptional in that it is the only entry in the data set, for which all astrometry was obtained after perihelion (Table 1). The object was actually discovered in the UV images, taken with the SWAN instrument on board the SOHO spacecraft, on 2004 April 29, 13 days before perihelion, according to three independent reports (Green 2004). The comet’s preperihelion absolute magnitude is extrapolated from the post-perihelion light curve on the assumption of its perihelion symmetry, given that there is no evidence of a major preperihelion outburst.

Comet C/2002 O4 (Hönl) is a difficult case. Nakano’s orbit in Table 1 shows a hyperbolic excess of nearly 40σ , more than for any other entry. From the observed evolution of tail orientation, Sekanina (2002) concluded that the comet was discovered in the course, possibly near the beginning, of an outburst that engulfed the entire nucleus, resulting in a significant fraction of its initial mass already lost by the time the event terminated. The peak post-outburst dust production rate, estimated at about 10^7 g s^{-1} , must have been much higher than the pre-outburst level. Analyzing Marsden’s orbital computations, Sekanina interpreted the gradually increasing hyperbolic excess as a corollary of progressive crumbling of the disintegrated nucleus. The comet’s pre-event absolute magnitude could not be derived from the light curve of the protracted outburst, leaving the discovery brightness estimate as the best possible source for a crude approximation.

The roots of the observed hyperbolic excess of the nine comets in Table 1 may differ from case to case. For the purpose of the present investigation I assume that all 20 comets with $(1/a)_{\text{orig}} < 0.000050 \text{ AU}^{-1}$ are members of the Oort Cloud.

C/2006 U1 is the most controversial entry in the set. With $(1/a)_{\text{orig}} = +0.000079 \text{ AU}^{-1}$ at 3σ , its orbit is on the inner outskirts of the Oort Cloud, so that there is a chance, however remote, that this is not an Oort Cloud comet. In fact, this comet may have made a number of revolutions about the Sun in the past and could have been, at its previous return to perihelion, diverted toward the Oort Cloud by the planetary perturbations, a scenario that is plausible in view of the random nature of the orbital-diffusion process. This possibility should be kept in mind, even though I formally list this object among the Oort Cloud comets.

Turning now to the examination of the survival status of the 20 Oort Cloud comets, I first point out that all those observed astrometrically for at least one to two months after perihelion are considered survivors (see Table 1). The remaining ones are disintegration suspects, and their status is, one by one, reviewed below.

To start with, C/2012 T5 was observed for position until 25 days after perihelion. However, closer inspection shows that this information is misleading, as the systematic monitoring of the comet’s motion terminated three weeks *before* perihelion. Only an isolated set of three astrometric positions was obtained after perihelion on a single night at the Observatoire de Dax (Code 958), which were not included by Nakano in his orbital solution. Ferrín (2014) reported that the comet’s light curve had features typical for the disintegrating comets. Kammerer (footnote 4) pointed out that the comet could not be detected visually after perihelion. Neither was it detected in CCD images 15 days after perihelion independently by H. Sato and M. Masek,⁵ having been fainter than magnitude 18, more than 9 mag fainter than three weeks before perihelion; the comet obviously perished.

The disintegration of C/2002 O7 (LINEAR) is apparent from a report by Mattiazzo (2003), whose CCD imaging showed the comet as a headless sunward-pointing tail of debris five days after perihelion. According to Tozzi et

al. (2003), the comet was fainter than magnitude 20.5, by more than 10 mag compared to its expected brightness, 72 days after perihelion.

C/2005 K2 split some 2.5 months before perihelion and four weeks before discovery (Sekanina 2005) and it flared up about 50 days later (Green 2005). A CCD image of the comet’s position taken by M. Mattiazzo (see footnote 5, message 8590) 27 days after perihelion revealed no object brighter than magnitude 16, a clear sign that the comet did not survive.

A consensus among visual and CCD comet observers was that C/2009 R1 (McNaught) stopped brightening several weeks before perihelion. The comet was very unfavorably located for observation near perihelion. J. Černý (see footnote 5, message 16773) reported repeatedly unsuccessful attempts to detect the comet over the period of more than three months post-perihelion with a 30-cm robotic telescope at the Pierre Auger Observatory, Malargüe, Argentina; subsequently he included the object among the extinct comets in his plot of light curves.⁶ Even though in this case the nature did not cooperate, I believe the evidence for disintegration is rather strong. Korsun et al. (2012) noted that the spectrum of this comet at an earlier time displayed an extremely low continuum, but strong molecular features.

The last astrometric observation of C/2011 M1 was made more than five weeks before perihelion in spite of favorable imaging conditions for another four weeks. The gap in the observations was apparently a consequence of the absence of a nuclear condensation, as implied by the observations made some 10 or so days before perihelion (see footnote 5, messages 17857–17859, 17862–17863, 17865–17866, and 17870–17872 that show a fuzzy, poorly condensed, “ghost” comet. The object was apparently not observed after perihelion, in spite of its increasing elongation to 30° by the time it was about 1.1 AU from the Sun. The evidence is compelling enough to deem this Oort Cloud member a nonsurvivor.

The intrinsically faint comet C/2016 U1, observed to within a day of perihelion passage (14° from the Sun!), showed no signs of fading. Starting five days after perihelion, it appeared for days in the SWAN images (see footnote 5, message 26174). It apparently was not seen from the ground, but it did not reach an elongation of 35° until nearly four months after perihelion. All signs point to the comet having survived perihelion essentially unscathed.

By contrast, C/2017 E4 was a quintessential example of a comet that perishes near perihelion. With the signature of its disintegration overwhelming, it is sufficient to document the case by referring to a paper by James (2017) that offers both the dynamical effect and imaging evidence of its demise.

With strong evidence against survival of the remaining Oort Cloud comets of interest — C/2002 O4, C/2010 X1 (Elenin), C/2012 S1 (ISON), and C/2017 S3 — as presented elsewhere (e.g., Sekanina 2002; Guido et al. 2011; Sekanina 2011; Ferrín 2014; Knight & Battams 2014; Sekanina & Kracht 2014; Li & Jewitt 2015; Sekanina & Kracht 2018), it is now possible to address the two major objectives of this investigation: (i) the dependence of perihelion survival (or failure to survive) of an Oort Cloud

⁵ Consult <https://groups.yahoo.com/neo/groups/comets-m1/conversations/messages/21071>.

⁶ See http://www.komet.cz/datas/users/ison+extinct_1.png.

Table 2
Oort Cloud Comets Arranged in Order of
Increasing Perihelion Distance

No.	Comet	Perihelion Distance, q (AU)	Absolute Magn., H_0	Survival Index, ΔH_{surv}	Observed Status
1	C/2012 S1	0.013	8.7	+1.6	Perished
2	C/2006 P1	0.171	6.2	-1.8	Survived
3	C/2017 S3	0.209	10.7	+2.4	Perished
4	C/2011 L4	0.302	5.4	-3.4	Survived
5	C/2016 U1	0.319	11.3	+2.4	<u>Survived</u>
6	C/2012 T5	0.323	11.0	+2.1	Perished
7	C/2009 R1	0.405	6.7	-2.7	<u>Perished</u>
8	C/2010 X1	0.483	8.6	-1.3	<u>Perished</u>
9	C/2017 E4	0.494	11.7	+1.7	Perished
10	C/2005 K2	0.545	13.5	+3.2	Perished
11	C/2002 T7	0.615	4.9	-5.8	Survived
12	C/2013 V5	0.625	8.6	-2.2	Survived
13	C/2002 O4	0.776	11	-0.7	<u>Perished</u>
14	C/2004 H6	0.776	7.4	-4.3	Survived
15	C/2015 G2	0.780	8.4	-3.3	Survived
16	C/2013 US ₁₀	0.824	4.9	-7.0	Survived
17	C/2007 W1	0.850	8.6	-3.5	Survived
18	C/2011 M1	0.896	9.5	-2.9	<u>Perished</u>
19	C/2002 O7	0.903	10.1	-2.3	<u>Perished</u>
20	C/2001 Q4	0.962	5.6	-7.2	Survived

comet on its perihelion distance and intrinsic brightness; and (ii) the degree of conformity of this relationship to Bortle’s (1991) formula for the survival limit. In relation to (ii) it should be remembered that (a) Bortle did not rule completely out survival of long-period comets fainter than the limit, only argued that the “likelihood of . . . surviving perihelion passage becomes drastically reduced”; (b) the absolute magnitudes H_0 that we use, based on Kammerer’s fit to visual observations, are not identical to H_{10} that Bortle used following the style of Vsekhsvyatsky (1958); typically for Oort Cloud comets, whose preperihelion variation with heliocentric distance r is less steep than r^{-4} (e.g., Whipple 1978), $H_0 < H_{10}$ at $r < 1$ AU and vice versa. Since the observed light curve for a comet with $q < 1$ AU often bridges the point at $r = 1$ AU, the difference between H_0 and H_{10} is usually insignificant; and (c) unlike Bortle, I distinguish between the Oort Cloud comets and other long-period comets with shorter orbital periods.

The Oort Cloud comets from Table 1 are arranged by increasing perihelion distance in Table 2. While columns 2–4 are copied from Table 1, the penultimate column lists a perihelion survival index, $\Delta H_{\text{surv}} = H_0 - H_{\text{surv}}$, introduced to test the *prediction* by Bortle’s formula. When $\Delta H_{\text{surv}} < 0$, the object is expected to survive, when $\Delta H_{\text{surv}} > 0$, it should perish. The last column indicates whether the comet was observed to survive or perish, as established in this section; if defying Bortle’s rule, the status is typed in boldface and is underlined to distinguish these objects from those that comply with the rule. The results are astonishing as they demonstrate that a whopping **50 percent of the Oort Cloud comets** with perihelia below 1 AU **perish!** Also, the relationship between the perishing comets and perihelion distance is stronger than expected: 70 percent of the objects with $q < 0.6$ AU and 30 percent with $0.6 < q < 1$ AU

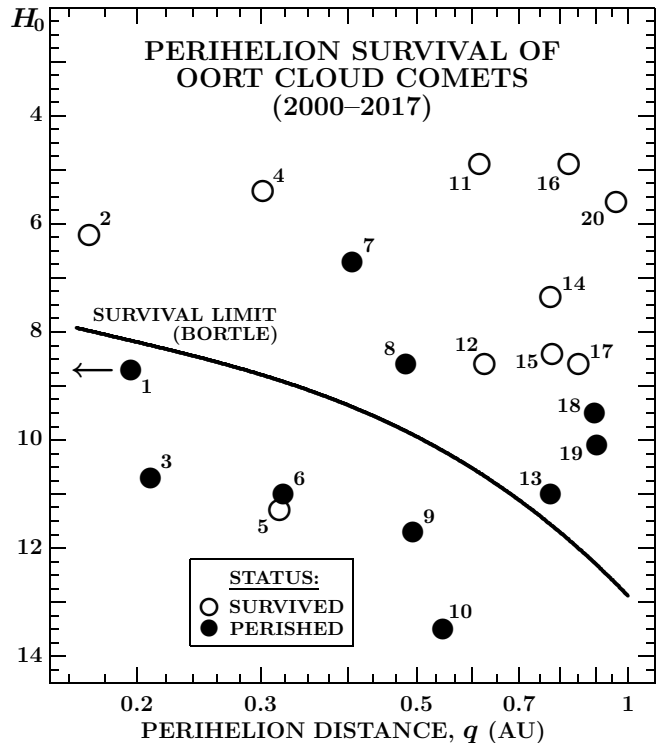


Figure 1. Oort Cloud comets discovered in 2000–2017 in the plot of the absolute magnitude H_0 against perihelion distance q . Open circles are the surviving objects, solid circles those perishing near perihelion. The comets are identified by their serial numbers from Table 2. Comets above the curve were predicted by Bortle (1991) to survive, below it to perish. The five perishing comets above the curve (Nos. 7, 8, 13, 18, and 19) show that the propensity of Oort Cloud comets for disintegration is stronger than expected. Only one comet, No. 5, survived while predicted to perish.

perish. These numbers are much higher than Bortle’s because of improved quality of the 2000–2017 observations. Besides the controversial comet C/2016 U1 there are only two survivors with small perihelion distances — C/2006 P1 (McNaught) and C/2011 L4 (PanSTARRS) — both spectacular and dust-rich comets (Section 6 and Table 6). The correlation with the absolute brightness is striking as well: only 14 percent of the Oort Cloud comets with $H_0 < 8$ perish but fully 86 percent with $H_0 > 10$ do so.

No less astounding are the results of comparison of the examined comets with Bortle’s formula; only one comet (the controversial C/2016 U1) survives in the region below the survival limit in Figure 1 (in fair agreement with Bortle’s expectation), but fully five perish — 36 percent among the comets expected to survive! Hence, **Bortle’s formula considerably underestimates the number of Oort Cloud comets that perish.**

5. COMETS WITH ORBITAL PERIODS OF 2000–1 000 000 YEARS

The procedure employed for the Oort Cloud comets was next applied to the comets of the other two categories defined at the end of Section 2, although no detailed description is provided of observational evidence on the status of the individual objects. It should be noted that for some of these comets it was more difficult than for the Oort Cloud comets to decide whether they survived or

Table 3
Comets With Orbital Periods 150 000–1 000 000 Years,
Arranged in Order of Increasing Perihelion Distance

No.	Comet	Perihelion Distance, q (AU)	Absolute Magn., H_0	Survival Index, ΔH_{surv}	Observed Status
1	C/2017 T1	0.581	12.3	+1.8	<u>Survived</u>
2	C/2009 O2	0.695	11.0	-0.2	<u>Perished</u>
3	C/2006 M4	0.783	6.5	-5.2	Survived
4	C/2003 T4	0.850	7.8	-4.3	Survived
5	C/2005 A1	0.907	8.2	-4.2	Survived

perished, primarily because of more limited data available. These complications notwithstanding, the validity of the main conclusions below is unaffected.

Consistent with dividing in Section 2 the non-Oort Cloud comets into two categories, the results are presented in Table 3 for the objects with the orbital periods longer than 150 000 years and in Table 4 with the orbital periods shorter than 50 000 years; the comets, for which it was possible to determine their survival status with less than full confidence, are tagged with a question mark and the entries are in the following assigned a weight of $\frac{1}{2}$.

The two tables show that, unlike for the Oort Cloud comets, only 12 percent of the comets in Tables 3–4 perished, and only 5 and 15 percent of those with perihelia below 0.6 AU and between 0.6 AU and 1 AU, did so, respectively. These numbers suffice to show the enormous differences relative to the main features of the Oort Cloud comets’ statistics. In particular, as is clearly illustrated

Table 4
Comets With orbital Periods 2000–50 000 Years, Arranged
in Order of Increasing Perihelion Distance

No.	Comet	Perihelion Distance, q (AU)	Absolute Magn., H_0	Survival Index, ΔH_{surv}	Observed Status
1	C/2002 V1	0.099	7.0	-0.6	Survived
2	C/2004 F4	0.168	8.3	+0.3	<u>Survived</u>
3	C/2002 X5	0.190	7.2	-0.9	Survived
4	C/2014 Q1	0.315	7.9	-1.0	Survived
5	C/2007 F1	0.402	8.3	-1.1	Survived
6	C/2016 R3	0.447	18	+8.3	Perished?
7	C/2014 C2	0.512	16	+4.7	<u>Survived</u>
8	C/2000 WM ₁	0.555	7.5	-2.8	Survived
9	C/2006 A1	0.555	8.5	-1.8	Survived
10	C/2006 WS ₄	0.591	16	+5.5	<u>Survived?</u>
11	C/2014 E2	0.664	6.8	-4.2	Survived
12	C/2015 C2	0.711	12	+0.7	<u>Survived</u>
13	C/2002 Y1	0.714	6.7	-4.6	Survived
14	C/2015 P3	0.715	14	+2.7	Perished?
15	C/2012 F6	0.731	5.2	-6.2	Survived
16	C/2001 A2	0.779	7.5	-4.2	Survived
17	C/2013 R1	0.812	7.1	-4.8	Survived
18	C/2017 T3	0.825	9.0	-3.0	Survived
19	C/2015 F3	0.834	16	+4.0	Perished
20	C/2011 C1	0.883	9.4	-2.9	Survived
21	C/2017 E1	0.901	10.5	-1.9	Survived
22	C/2016 VZ ₁₈	0.910	18	+5.5	<u>Survived</u>
23	C/2007 T1	0.969	7.7	-5.1	Survived

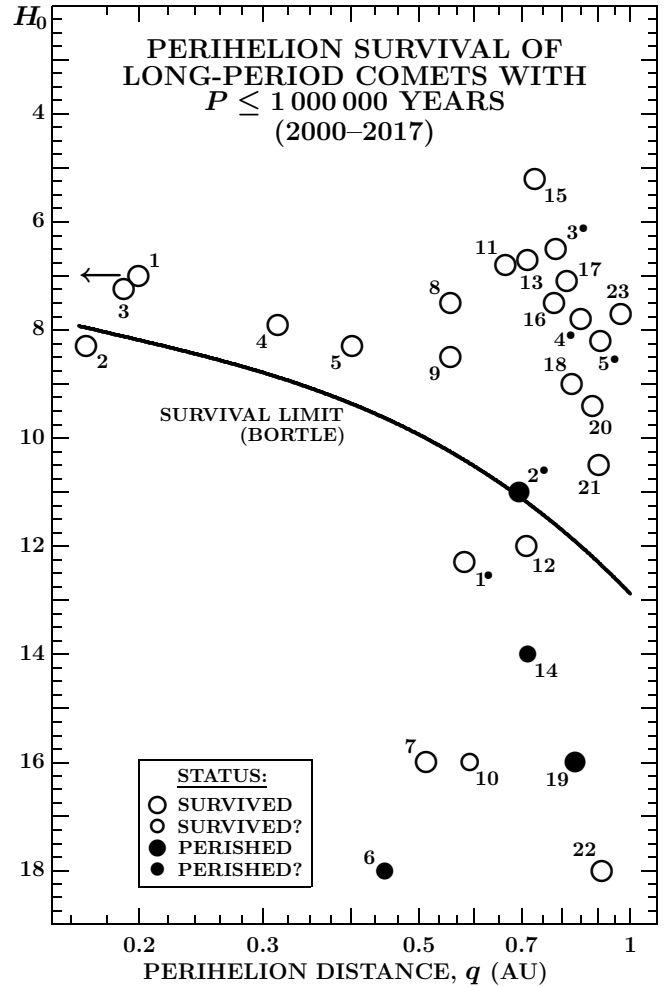


Figure 2. Long-period comets, not belonging to the Oort Cloud, discovered in 2000–2017 in the plot of the absolute magnitude H_0 against perihelion distance q . Open circles of two different sizes represent objects observed to have survived (larger symbols) or possibly survived perihelion, solid circles of two different sizes show comets that perished (larger symbols) or possibly perished near perihelion. The individual objects are identified by their serial numbers listed in Tables 3 and 4, the ones from Table 3 are distinguished by a superscript dot following the digit. It is noted that, contrary to the Oort Cloud comets in Figure 1, an overwhelming majority of these comets survive, showing no correlation with the survival limit curve whatsoever.

in Figure 2, the fraction of perished comets is substantially depressed and the dependence of their numbers on perihelion distance tend to be, if anything, reversed, increasing rather than decreasing with q . On the other hand, only about 25 percent of these comets defy Bortle’s rule, nearly all in the sense Bortle anticipated (i.e., with surviving comets below the threshold line).

To summarize the results of this section, the **non-Oort Cloud long-period comets nearly all survive**. This category of comets appears to have dominated the data set employed by Bortle (1991), as comparison with the entries in Tables 3 and 4 suggests.

For the sake of completeness I present, in Table 5, the 12 comets in parabolic and poorly determined elliptic orbits (Section 2). Most of them were observed over very short arcs of their orbits and they offer no meaningful information on their perihelion survival status.

Table 5

Comets With Parabolic or Poorly Determined Elliptic Orbits, Arranged in Order of Increasing Perihelion Distance

No.	Comet	Perihelion Distance, q (AU)	Absolute Magn., H_0	Survival Index, ΔH_{surv}	Observed Status
1	C/2004 R2	0.113	10	+2.3	Perished
2	C/2004 V13	0.181	7.2	-0.9	<u>Perished?</u>
3	C/2000 W1	0.321	10.2	+1.3	<u>Survived?</u>
4	C/2002 F1	0.438	9.8	+0.2	<u>Survived</u>
5	C/2008 J4	0.448	16	+6.3	Perished
6	C/2002 O6	0.495	9.7	-0.3	<u>Perished</u>
7	C/2000 S5	0.605	9.8	+1.3	Perished?
8	C/2010 F4	0.614	14	+3.3	?
9	C/2004 S1	0.679	20	+8.9	Perished?
10	C/2012 C2	0.801	12.0	+0.2	Perished
11	C/2013 G5	0.928	20	+7.4	Perished
12	C/2013 K1	0.949	18	+5.3	<u>Survived?</u>

6. REVISION OF PERIHELION SURVIVAL LIMIT FOR OORT CLOUD COMETS

The results of the preceding sections indicate that the **nuclei of Oort Cloud comets differ dramatically in their behavior near the Sun from the nuclei of other long-period comets**. The Oort Cloud comets account for virtually all instances of disintegration reported by observers to begin as early as several weeks before perihelion and manifested by the sudden loss of the nuclear condensation usually, but not always, after a brief flare-up. There is also evidence that most, if not all, of the perishing comets are poor dust producers.

The finding that it is *only* the Oort Cloud comets that have this strong propensity for perishing near perihelion provides a critical piece of evidence for the hypothesis that an **interstellar comet** of comparable physical properties **should have suffered a similarly debilitating incident** shortly before perihelion, **with 1I/‘Oumuamua emerging as its debris**. An argument that a sizable fragment could never survive the disintegration process is countered by referring to Li & Jewitt’s (2015) study on one such event, experienced by C/2010 X1; they were so struck by the lack of vigor of the episode that they described the disappearing comet — in their paper’s title — as “gone with a whimper, not a bang”.

Observations suggest that the process of disintegration of an Oort Cloud comet is strongly perihelion-distance dependent. While a comprehensive modeling of the conditions necessary for the nucleus’ perihelion survival is beyond the scope of this paper, it appears that on its approach to perihelion a **comet perishes because it fails to control effects of the steeply accelerating rate of increase in the incident solar radiation flux, \mathcal{F}_\odot** — as if getting overheated. I accept the rate of flux increase as a proxy of the force that imperils the comet’s survival. At time t before the perihelion passage t_π ($t < t_\pi$), when the comet’s heliocentric distance is r , the rate of increase in the incident solar flux is

$$\dot{\mathcal{F}}_\odot(t) = \frac{d}{dr} \left(\frac{\mathcal{F}_0}{r^2} \right) \cdot \frac{dr}{dt}, \quad (1)$$

where \mathcal{F}_0 is the solar constant and dr/dt can for Oort Cloud comets be expressed with sufficient accuracy by a

parabolic approximation,

$$t = t_\pi - \frac{\sqrt{2}}{3k} (r+2q)\sqrt{r-q}, \quad (2)$$

with k being the Gaussian gravitational constant. The rate of increase in the solar flux is then given by

$$\dot{\mathcal{F}}_\odot(t) = \sqrt{8} k \mathcal{F}_0 r^{-\frac{7}{2}} \sqrt{1 - \frac{q}{r}}, \quad (3)$$

which implies $\dot{\mathcal{F}}_\odot(t_\pi) = 0$ and reaches a maximum of

$$(\dot{\mathcal{F}}_\odot)_{\text{max}} = \left(\frac{7}{8} \right)^{\frac{7}{2}} k \mathcal{F}_0 q^{-\frac{7}{2}} = C_0 q^{-\frac{7}{2}} \quad (4)$$

at $r_{\text{max}} = \frac{8}{7} q$, or at

$$t_{\text{max}} = t_\pi - \frac{22}{21k} \sqrt{\frac{2}{7}} q^{\frac{3}{2}} = t_\pi - 32.55 q^{\frac{3}{2}}, \quad (5)$$

where C_0 is a constant; time is in days when q is in AU. The process of disintegration is completed before t_{max} , if it needs $\dot{\mathcal{F}}_\odot < (\dot{\mathcal{F}}_\odot)_{\text{max}}$; it may continue after t_{max} , even after perihelion passage, depending on the degree of inertia. For strongly hyperbolic orbits, see Appendix A.

Comets can cope with a high rate of increase in the incident solar flux in a variety of ways. Short-period comets with small perihelion distance, such as 96P/Machholz or 2P/Encke, as well as long-period comets with many perihelion passages in their past, such as C/2002 V1 or C/2004 F4, have long had the opportunity to build up a surface mantle of sintered dust to improve strength. Deprived of this option, Oort Cloud comets have to resort to revving up their outgassing; when almost all incident radiation is spent on the sublimation of ices, the surface temperature is kept nearly constant during approach to perihelion. Observations of Oort Cloud comets indicate that this response to increasing solar radiation works well at heliocentric distances greater than ~ 1 AU. At about this point in the orbit, however, the objects’ brightness is reported to grow at a progressively slower rate and eventually to stall, an apparent sign that the nucleus is running out of near-surface supplies of ice. The inevitable consequence of this ice repository’s exhaustion is the promptly increasing surface temperature, with the undesirable implications, such as surface material’s thermal expansion, an upsurge in the associated thermal stress, etc. The deteriorating conditions cannot long be accommodated by the devolatilized surface. If the comet happens to reach perihelion in the meantime, it might survive, otherwise it surely disintegrates.⁷ The likelihood of survival depends strongly on the perihelion distance, varies from object to object, and is described by an accommodation limit \mathcal{A} . When a comet of perihelion distance q is on the verge of disintegration, one has

$$\mathcal{A} = (\dot{\mathcal{F}}_\odot)_{\text{max}} = C_0 q^{-\frac{7}{2}}. \quad (6)$$

Observations of Oort Cloud comets further indicate, as already pointed out, that the perihelion survival limit is a function of the comet mass, \mathcal{M} : brighter (and presumably more massive) comets appear to be able to tolerate

⁷ The disintegration (loss of the nuclear condensation) is sometimes preceded by a brief flare-up, apparently the evidence that a reservoir of ice deep in the nucleus’ interior was being tapped.

Table 6
Oort Cloud Comets Arranged in Order of Decreasing Synoptic Index $\mathfrak{S}_{\text{surv}}$

No.	Comet	Perihelion Distance, q (AU)	Absolute Magnitude, H_0	Dust Proxy $\log(Af\rho)_0$ (cm)	Synoptic Index, $\mathfrak{S}_{\text{surv}}$	Observed Status
1	C/2012 S1	0.013	8.7	2.6 ^a	+9.7	Perished
2	C/2005 K2	0.545	13.5	1.4	+7.0	Perished
3	C/2016 U1	0.319	11.3	1.3	+6.3	Survived
4	C/2012 T5	0.323	11.0	1.4	+5.8	Perished
5	C/2017 S3	0.209	10.7	2.0	+5.6	Perished
6	C/2017 E4	0.494	11.2	1.4	+5.5	Perished
7	C/2002 O4	0.776	11	2.5	+1.8	Perished
8	C/2011 M1	0.896	9.5	1.6	+1.4	Perished
9	C/2009 R1	0.405	6.7	1.5 ^b	+0.8	Perished
10	C/2010 X1	0.483	9.6	2.4	+0.7	Perished
11	C/2002 O7	0.903	10.1	2.4	+0.6	Perished
12	C/2007 W1	0.850	8.6	2.2	-0.3	Survived
13	C/2004 H6	0.776	7.4	2.0	-1.0	Survived
14	C/2013 V5	0.625	8.6	3.1	-1.1	Survived
15	C/2006 P1	0.171	6.2	3.9	-1.5	Survived
16	C/2015 G2	0.780	9.4	3.0	-1.7	Survived
17	C/2011 L4	0.302	5.4	4.3 ^c	-4.4	Survived
18	C/2002 T7	0.615	4.9	3.0 ^d	-4.6	Survived
19	C/2001 Q4	0.962	5.6	3.1	-5.2	Survived
20	C/2013 US ₁₀	0.824	4.9	4.3 ^e	-7.5	Survived

Notes.

^a From Moreno et al. (2014).

^b Scaled from results by Borisov et al. (2012); supported by Korsun et al.’s (2012) findings.

^c Scaled from results by Opitom et al. (2013).

^d Scaled from results by Rosenbush et al. (2006).

^e Scaled from result by Protopapa et al. (2018).

higher rates of increase in the solar flux than fainter (less massive) comets. Accordingly,

$$\mathcal{A} \propto \mathcal{M} = c_0 10^{-\frac{3}{5}H_0}, \quad (7)$$

where the absolute magnitude H_0 is assumed to vary as the nucleus’ surface area and the nucleus’ mass as a power of $\frac{3}{2}$ of the surface area; $c_0 = 2.5 \times 10^{19}$ g according to Whipple (1975). Comparing relations (6) and (7), one obtains a relationship between the perihelion distance and the absolute magnitude that offers a condition for the perihelion survival limit:

$$H_0 = c + \frac{35}{6} \log q, \quad (8)$$

where c is a constant. Comparison with the data points in Figure 1 shows that this relation, like Bortle’s formula, fails to discriminate between a number of surviving and perishing comets, implying that the condition for the perihelion survival limit is more complex.

It is the particulate dust in the atmosphere of an Oort Cloud comet that makes the difference. Dust-rich comets are more resistant than dust-poor comets to damage from effects of a high rate of solar-flux increase. As the rate of injection of dust from the nucleus increases, the comet’s atmosphere grows progressively less transparent, until it eventually becomes optically thick, thereby protecting the nucleus against further heating.

The accommodation limit \mathcal{A} ought to show this aptitude of dustier comets. Since the rate of dust injection $\dot{\mathcal{M}}_d$ and its variation with heliocentric distance, r^{-m} , are

seldom known for Oort Cloud comets, I replace $\dot{\mathcal{M}}_d$ with a more readily available proxy quantity $Af\rho$, introduced by A’Hearn et al. (1984), extensively examined by Fink & Rubin (2012), and related to $\dot{\mathcal{M}}_d$ by

$$\dot{\mathcal{M}}_d(r) = (\dot{\mathcal{M}}_d)_0 r^{-m} = C_d (Af\rho)_0 r^{-m}, \quad (9)$$

where $(\dot{\mathcal{M}}_d)_0$ and $(Af\rho)_0$ are, respectively, the dust injection rate and the dust parameter at 1 AU from the Sun, and C_d is a conversion coefficient that depends on the particle-size distribution function. With the quantity $Af\rho$ to be expressed in cm, the improved model suggests for the accommodation limit \mathcal{A}

$$\mathcal{A} \propto \mathcal{M} \cdot (\dot{\mathcal{M}}_d)_0 \propto 10^{-\frac{3}{5}H_0} \cdot (Af\rho)_0. \quad (10)$$

The condition (8) now changes to

$$H_0 = a + \frac{35}{6} \log q + \frac{5}{3} \log (Af\rho)_0. \quad (11)$$

The last step in testing this procedure is the introduction of a **synoptic index for perihelion survival**, $\mathfrak{S}_{\text{surv}}$, by rearranging Eq. (11) and choosing $a = 5.7$, so that, similarly to ΔH_{surv} , $\mathfrak{S}_{\text{surv}} < 0$ when a comet is predicted to survive perihelion essentially intact and $\mathfrak{S}_{\text{surv}} > 0$ when it is predicted to perish:

$$\mathfrak{S}_{\text{surv}} = H_0 - 5.7 - \frac{35}{6} \log q - \frac{5}{3} \log (Af\rho)_0. \quad (12)$$

The 20 Oort Cloud comets from Table 2, rearranged by decreasing index $\mathfrak{S}_{\text{surv}}$, are listed in Table 6. Columns 2 to 4 are copied from Table 2, whereas $(Af\rho)_0$ in column

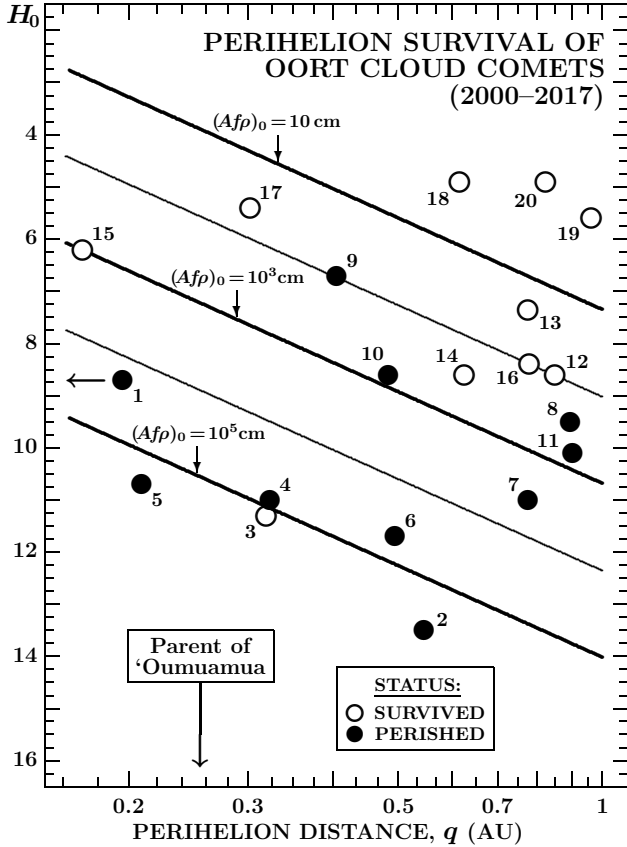


Figure 3. Oort Cloud comets discovered in 2000-2017 in the plot of the absolute magnitude H_0 against perihelion distance q , with the lines of a constant normalized dust parameter $(Af\rho)_0$ between 10 cm and 10^5 cm. The comets are identified by their serial numbers from Table 6. Only the controversial comet C/2016 U1 (No. 3) does not fit the three dimensional relationship among q , H_0 , and $(Af\rho)_0$. Also marked in the plot is the position of ‘Oumuamua’s parent. See the caption to Figure 1 for more explanation.

5 has extensively been researched in the literature. For most entries in the table the starting value was taken from the Spanish website maintained by J. Castellano, E. Reina, and R. Naves.⁸ For five comets the starting data were taken from other sources, listed in the footnotes to Table 6. The value of $Af\rho$ at ~ 1 AU from the Sun was used when available, otherwise the value closest to 1 AU. If a series of data over a fairly wide interval of heliocentric distances showed that $Af\rho$ was essentially constant then this value was identified with $(Af\rho)_0$; if not, the tabulated value was reduced to 1 AU assuming an r^{-2} variation. The resulting value of $(Af\rho)_0$ was then normalized to a zero phase angle employing either the dust-rich or dust-poor version of the model developed by Marcus (2007). It is this value that is listed in column 5 of Table 6. Column 6 presents the index $\mathfrak{S}_{\text{surv}}$ computed from Eq. (12) and column 7, again copied from Table 2, allows one to compare the prediction based on $\mathfrak{S}_{\text{surv}}$ with each comet’s actual status.

Except for the controversial object C/2016 U1, this new index $\mathfrak{S}_{\text{surv}}$ correctly discriminates between the surviving and perishing comets. One immediately notices a strong concentration of the intrinsically faint and dust

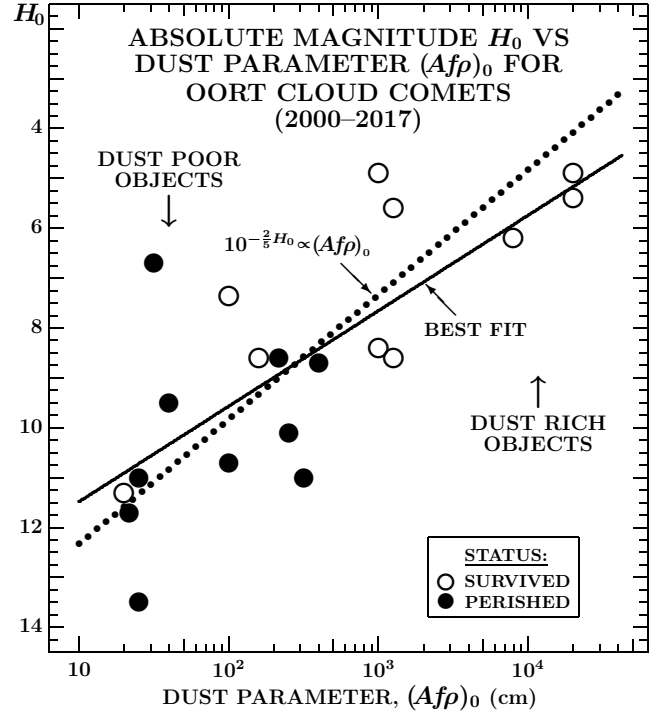


Figure 4. Plot of the absolute magnitude H_0 against the dust parameter $(Af\rho)_0$ for the 20 Oort Cloud comets discovered between 2000 and 2017. The surviving and perishing objects are again represented by different symbols. The dotted line is a fit expected on the assumption that both the absolute brightness and the dust production rate vary as the surface area of the nucleus. Striking is a concentration of the perishing comets, mostly intrinsically faint and dust poor, to the lower left, whereas the surviving comets, mostly bright and dust rich, are to the upper right.

poor comets toward the top of the table, while the bright and dust rich comets heavily prevail near the bottom.

The introduction of $Af\rho$ allows one to represent the perihelion survival limit ($\mathfrak{S}_{\text{surv}} = 0$) in the plot of H_0 against $\log q$ as a system of parallel straight lines shown in Figure 3. An object is predicted to survive perihelion when located above the line with the respective value of $(Af\rho)_0$, but to perish when below the line. For example, C/2005 K2 (No. 2) and C/2017 S3 (No. 5) are predicted to perish even if their $(Af\rho)_0$ was as high as 10^5 cm, whereas C/2002 T7 (No. 18), C/2001 Q4 (No. 19), and C/2013 US₁₀ (No. 20) are predicted to survive even if their $(Af\rho)_0$ was as low as 10 cm.

Also marked in Figure 3 is the position of the parent comet of ‘Oumuamua. From the nondetection in the June 2017 PanSTARRS images I estimated its peak absolute magnitude at $H_0 \gtrsim 18$ (Sekanina 2019). If similar to Oort Cloud comets in morphology and other physical properties, the **near-perihelion disintegration of ‘Oumuamua’s parent is absolutely inevitable.**

The complete dominance of intrinsically bright and dust-rich Oort Cloud comets among the perihelion survivors is likewise illustrated in a plot of the absolute magnitude against the dust parameter $(Af\rho)_0$, displayed in Figure 4. Accepting an assumption that both the dust production rate and the intrinsic brightness vary as the surface area of the nucleus, one would expect that

$$H_0 = b - 2.5 \log(Af\rho)_0, \quad (13)$$

⁸ See <http://astrosurf.com/cometas-obs>.

Table 7
List of Oort Cloud Comets Discovered in 1989–1999 Whose Perihelion Distances Are Less Than 1 AU^a

Comet	Time of Perihelion, t_π (TT)	Perihelion Distance, q (AU)	Reciprocal Semimajor Axis ^b , $(1/a)_{\text{orig}}$ (AU ⁻¹)	Orbital Arc Observed (d)			Abs. Magn., H_0	Surv. Limit, H_{surv}	Reference
				Δt_{obs}	Δt_{beg}	Δt_{last}			
C/1989 Q1	1989 Nov 11.9	0.642	-0.000218 ± 0.000022	122.0	-79.4	+42.6	7.1	10.9	Marsden ^c
C/1989 X1	1990 Apr 10.0	0.350	$+0.000032 \pm 0.000002$	202.9	-124.3	+78.6	5.6	9.1	MPC ^d
C/1991 X2	1992 Mar 21.2	0.199	$+0.000057 \pm 0.000154$	80.9	-98.7	-17.8	10.1	8.2	MPC ^{d,e}
C/1991 Y1	1992 Feb 01.0	0.644	-0.000094 ± 0.000006	130.0	-38.6	+91.4	8.8	10.9	MPC ^d
C/1993 Q1	1994 Mar 26.3	0.967	$+0.000003 \pm 0.000003$	566.2	-544.0	+22.2	7.4	12.8	MPC ^d
C/1996 N1	1996 Aug 03.4	0.926	-0.000153 ± 0.000006	122.5	-30.0	+92.5	8.0	12.6	Muraoka ^{f,g}
C/1999 S4	2000 Jul 26.2	0.765	$+0.000003 \pm 0.000002$	308.5	-302.8	+5.7	8.9	11.6	Muraoka ^{f,h}

Notes.

^a For explanation of individual columns, see notes to Table 1

^b Referred to barycenter of Solar System. All original orbits derived from gravitational osculating orbits.

^c See Marsden (1990).

^d See footnote 3.

^e Questionable member of Oort Cloud because of large uncertainty in $(1/a)_{\text{orig}}$.

^f See footnote 1.

^g Nearly identical orbit derived by Nakano (1996).

^h Nearly identical orbit derived by Marsden (2000b).

where b is a constant. Fitting the 20 Oort Cloud comets from 2000–2017 to this relation yields $b = 14.8 \pm 1.8$. On the other hand, the best least-squares fit is

$$H_0 = 13.4 - 1.9 \log(Af\rho)_0. \quad (14)$$

$$\pm 1.1 \pm 0.4$$

The modest difference between (13) and (14) is caused by scatter among individual comets; for example, removing C/2009 R1 changes the slope to -2.15 ± 0.37 .

7. EXAMINING EARLIER OORT CLOUD COMETS

There were reasons for limiting this investigation to the period of time beginning in 2000. Nakano’s series of high-accuracy orbit determination with a full display of positional residuals focused almost exclusively on short-period comets before 2000; Kammerer started his catalog of light curves with the comets of 1997; and the collection of the parameter $Af\rho$ in the Spanish website dates back — with very few exceptions — to 1999.⁹

Nonetheless, since Bortle’s set of long-period comets ended with the 1988 objects, I considered it appropriate that this study include a condensed report on the Oort Cloud comets from the intervening period of 1989–1999.

The procedure that was employed to compile Table 1 was now used to present a set of the Oort Cloud comets from this 11-year span with orbits of known quality. The results of this effort in Table 7 show that the number of such dynamically new comets between 1989 and 1999 totals seven at best, as one of them is burdened with an error so large that its aphelion distance is entirely indeterminate, even though the nominal value places the comet near the inner boundary of the Oort Cloud. The remaining six entries are secure, the original orbits always determined from gravitational solutions, despite the shorter orbital arcs that had to be used (to avoid systematic trends in the residuals), thus involving larger formal

errors than misleading results based on nongravitational solutions would imply. The light curves of the seven comets and their parameters were published by Machholz (1994, 1996) and by Shanklin (1997, 1998, 2001, 2009). An overlap of Shanklin’s (2009) and Kammerer’s (footnote 4) light curves in 1999 shows they are in excellent agreement with one another.

The 1989–1999 collection, which delivers only marginally more than just one Oort Cloud comet per two years (compared to more than one per year in the 2000–2017 period), is incomplete, as several additional likely members of the Oort Cloud are, judging from their physical behavior, cataloged among the comets with parabolic orbits — the same problem that Bortle was confronted with to a much greater extent in his 1800–1988 orbital data set.

Chronologically the first of the 1989–1999 Oort Cloud comets, C/1989 Q1 (Okazaki-Levy-Rudenko; old designation 1989r = 1989 XIX), was observed for astrometry over a post-perihelion period of more than 40 days, visually for nearly 8 weeks. Observations of $Af\rho$ were reported by A’Hearn et al. (1995) and the original orbit was computed by Marsden (1990). Even though the post-perihelion fading was steeper than the preperihelion brightening (common among Oort Cloud comets), the comet became more condensed as it neared perihelion and retained this appearance until the end of observations (Machholz 1996), showing no sign of disintegration whatsoever.

The next comet in the table, C/1989 X1 (Austin; old designation 1989c₁ = 1989 V), was observed for about eleven weeks after perihelion, despite its steeper post-perihelion fading, similar to that of C/1989 Q1 (Machholz 1994). Data on $Af\rho$ were reported by Schleicher & Osip (1990), by Osip et al. (1993), and by A’Hearn et al. (1995). There are no doubts that the comet survived perihelion.

A different story is C/1991 X2 (Mueller; old designation 1991h₁ = 1992 VIII), whose astrometric and visual

⁹ On the other hand, a set of 85 comets by A’Hearn et al. (1995), incomplete as it is, terminates in 1992.

Table 8
Comparison of Survival Index ΔH_{surv} with Synoptic Index $\mathfrak{S}_{\text{surv}}$ for Oort Cloud Comets
from 1989–1999 Arranged by Increasing Perihelion Distance

No.	Comet	Perihelion Distance, q (AU)	Absolute Magnitude, H_0	Dust Proxy $\log(Af\rho)_0$ (cm)	Survival Index, ΔH_{surv} ^a	Synoptic Index, $\mathfrak{S}_{\text{surv}}$	Observed Status
1	C/1991 X2	0.199	10.1	...	+1.9	Perished ^b
2	C/1989 X1	0.350	5.6	3.0	-3.5	-2.4	Survived
3	C/1989 Q1	0.642	7.1	2.7	-2.8	-2.0	Survived
4	C/1991 Y1	0.644	8.8	>2.3	-2.1	<+0.4 ^c	Survived
5	C/1999 S4	0.765	8.9	2.2	-2.7	+0.2	Perished
6	C/1996 N1	0.926	8.0	...	-4.6	Survived ^d
7	C/1993 Q1	0.967	7.4	...	-5.4	Perished ^e

Notes.

^a Typed in italics when predicts incorrect status.

^b Requires $(Af\rho)_0 < 10^{5.1}$ cm to make $\mathfrak{S}_{\text{surv}} > 0$; undoubtedly satisfied.

^c Inconclusive.

^d Requires $(Af\rho)_0 > 10^{1.5}$ cm to make $\mathfrak{S}_{\text{surv}} < 0$.

^e Requires $(Af\rho)_0 < 10^{1.1}$ cm to make $\mathfrak{S}_{\text{surv}} > 0$.

observations were terminated nearly three weeks before perihelion because of the comet’s rapidly decreasing elongation. No information on $Af\rho$ appears to be available. Within three weeks after perihelion, the comet was unsuccessfully searched for in the infrared (Gehrz 1992) as well as at optical wavelengths (Hale 1992; Kobayashi 1992; Seki 1992). Shanklin (1997) concluded that the comet had failed to survive. The observed arc of the orbit is too short to determine a set of high-quality elements (MPC; see footnote 3), so the comet’s Oort Cloud membership is uncertain, even though its near-perihelion disappearance provides an argument to the contrary.

Discovered only 10 days later, C/1991 Y1 (Zanotta-Brewington; old designation 1991g₁ = 1992 III) was a survivor, despite its asymmetric light curve with a steeper post-perihelion fading (Shanklin 1997). The only $Af\rho$ data for this comet were obtained by Jorda et al. (1995), unfortunately after perihelion. The conversion to the normalized preperihelion value to be used in the expression for the synoptic index is burdened by large uncertainties, in part because at the time of Jorda et al.’s observation the comet’s brightness already subsided dramatically. Under the circumstances, I only could try to estimate a lower limit to the necessary correction. The astrometry was obtained over a period of three months after perihelion and the comet’s survival is indisputable.

A peculiar case is C/1993 Q1 (Mueller; old designation 1993p = 1994 IX), which continued to brighten for two weeks past its perihelion near 1 AU. The last astrometric observation was made about one week later. Only at that point in the orbit did the comet’s appearance suddenly changed; the disappearance of the nucleus’ condensation and dramatic fading were reported by Gilmore (1994) on exposures taken 39–40 days after perihelion and by Camilleri (1994) visually a week later, and confirmed by Scotti (1994) by images taken another three or so weeks later.

Comet C/1996 N1 (Brewington), discovered only one month before perihelion, experienced an outburst of 1 mag in amplitude five days after perihelion. The event was not, however, followed by the loss of nuclear condensation, perhaps in part because of the perihelion dis-

tance that exceeded 0.9 AU. The comet was observed for astrometry for three months after perihelion and the indications are that it survived.

The last member of this group of 1989–1999 comets, C/1999 S4 (LINEAR), was a major surprise. I return to the dramatic changes in the comet’s appearance and the implications in Section 8; here I only note that, in spite of its relatively large perihelion distance, the comet did undergo a flare-up a few days before perihelion, followed by the ominous disappearance of the nucleus’ condensation. The difference compared to many previous (as well as subsequent) similar occasions is that the events evolving *after* the flare-up’s termination were under scrutiny with the help of the Hubble Space Telescope (HST) and the Very Large Telescope (VLT), then the most powerful ground-based instrument (Weaver et al. 2001). The condensation’s “disappearance” turned out under this in-depth view to consist of more than a dozen mini-comets that were being rapidly deactivated, the foolproof evidence that the comet had perished. The $Af\rho$ data were measured and studied extensively by Farnham et al. (2001) and by Bonev et al. (2002); the data from a broad range of heliocentric distances were averaged to derive an effective value.

The observed status of the 1989–1999 Oort Cloud comets, arranged by increasing perihelion distance, is in Table 8 compared with both indices, ΔH_{surv} and $\mathfrak{S}_{\text{surv}}$. The synoptic index could not be evaluated for three objects and only constrained for a fourth one because of missing or incomplete data. The table shows that the index ΔH_{surv} predicts survival (typed in italics) for two perished comets, C/1993 Q1 and C/1999 S4, a fraction of the set similar to that in the 2000–2017 collection.

8. MORPHOLOGY AND SIZE OF DEBRIS LEFT BEHIND BY PERISHED OORT CLOUD COMETS

Reports on the appearance of most perished Oort Cloud comets in their final stage of development are limited to acknowledging that they either completely vanished or turned into a barely detectable diffuse cloud with no evidence of a nucleus’ condensation. There are only four instances with some information provided on

what did the process of “disappearance” mean in terms of the dimensions of the surviving debris, with a potential of application to ‘Oumuamua: C/1999 S4, C/2010 X1, C/2012 S1, and C/2017 S3.

The most extensive amount of information was collected for C/1999 S4, which was observed by the Hubble Space Telescope (HST) even before it began to show the clear signs of disintegration (Weaver et al. 2001). Three weeks before perihelion the brightness of the innermost coma (within 100 km of the nucleus) exhibited major variations on a time scale of tens of hours, possibly associated with the release of a small fragment. The light curve reached a broad maximum at about this time, but a gradual decline was suddenly interrupted by a sharp flare-up, peaking three days before perihelion, confirmed by an analysis of the dust tail (Weaver et al. 2001) and coinciding with a peak in the production of water (Mäkinen et al. 2001). Two days later the coma became clearly cigar shaped (Kidger 2002), rapidly developing into a long dust tail with a relatively sharp tip devoid of any condensation in the ground-based observations. Closeup imaging of this tip by the HST 10 days after perihelion revealed a cluster of more than a dozen fragments, each resembling a miniature comet with its own coma and tail. Some 37 hours later the head of the comet was imaged with the Very Large Telescope (VLT) to show about 16 fragments. A photometric and dynamical investigation of the HST and VLT images showed that the fragments were 50 to 120 meters in diameter (assuming a geometric albedo of 4 percent), at least some of them released long before perihelion, and typically subjected to non-gravitational accelerations, probably outgassing driven, of about 10×10^{-8} AU day⁻² (Weaver et al. 2001), less than 50 percent of the nongravitational acceleration affecting the orbital motion of ‘Oumuamua. Significantly, no fragments were detected in the VLT images taken 12 and 17 days after perihelion, i.e., 15 and 20 days after the terminal flare-up, fading by a factor of 2 to 10 in 72 hours. An obvious conclusion is that the disintegration process of C/1999 S4 proceeded very rapidly. The comet’s surviving dust tail was detected by G. J. Garradd¹⁰ with his 45-cm f/5.4 reflector two weeks after the last VLT detection of the fragments.

The sublimation area of C/1999 S4, determined from the water production rates by Mäkinen et al. (2001) based on their SWAN observations over a period from two to one month before perihelion, amounts to 1.4 km², while the nucleus’ projected area derived on the assumption of a spherical nucleus from the nongravitational acceleration affecting the comet’s orbital motion (Marsden & Williams 2008) is at most 0.5 km². This enormous disparity implies that even *before* the disintegration event the nucleus may have been strongly nonspherical; the assumption of a pancake-like shape leads to a long-to-short dimension ratio of about 5.5, reminiscent of ‘Oumuamua’s inferred shape. Alternatively, the nucleus may have been very “fluffy”, with the effective bulk density much lower than assumed, thereby compromising the determination of the projected area from the mass of the dynamical model, an issue that is also highly relevant to ‘Oumuamua.

With a perihelion distance substantially smaller than C/1999 S4, comet C/2010 X1 experienced a flare-up more than three weeks before perihelion (Li & Jewitt 2015; Sekanina 2011) and almost immediately began to lose the nucleus’ condensation (Mattiazzo & McNaught 2011). Li & Jewitt (2015) illustrate the dramatic change in the comet’s appearance imaged with the same telescope five weeks apart in their Figure 4. The comet was too close to the Sun in the sky for ground-based observing from shortly before perihelion until one month after perihelion. Li & Jewitt used the 360-cm CFHT reflector to image the comet’s expected position 40 days after perihelion, but without success. They estimated that any potentially surviving fragments could not be larger than 80 meters across. Much larger upper limit on the size of nuclear fragments was reported by Kidger et al. (2016) from their negative observations with the Herschel Space Observatory.

Comet C/2012 S1 was an extreme case because of the exceptionally small perihelion distance of 2.7 solar radii. Rather than providing a summary of the various investigations published on this comet, I paraphrase Sekanina & Kracht’s (2014) proposed timeline of events, based on such studies. This time interval began 16 days before perihelion at a heliocentric distance of 0.7 AU with a minor increase in the water production that was followed by a major outburst, when the production went up by a factor of 16. This surge suggested that a new source of water was tapped, requiring fragmentation of the nucleus. A few days later there was another production jump, by a factor of three, implying further fragmentation. Then about three days before perihelion came a dramatic drop in the gas production, suggesting that the comet’s reservoir of ice was practically exhausted. The comet *de facto* ceased to exist already at this time, except that the sublimation of sodium was still increasing and the process of cascading fragmentation continuing. All post-perihelion images taken by the coronagraphs on board the SOHO and STEREO spacecraft consistently show that dust was ejected from nuclear fragments until 3.5 hours before perihelion, when at 5 solar radii the process had nothing to feed itself on any more — the ultimate termination of activity. While Knight & Bataams (2014) estimated “any remaining active nucleus [at] < 10 meters in radius”, Sekanina & Kracht’s (2014) scenario led them to the conclusions that the largest surviving *inert fragments* of the nucleus were at best pebble sized and that *no active* nucleus survived, a notion supported by Curdt et al.’s (2014) failure to find any Lyman-alpha emission less than one hour before perihelion.

Comet C/2017 S3 underwent two preperihelion outbursts; the first began nearly seven weeks before perihelion at a heliocentric distance of 1.25 AU, the second two weeks later at 0.96 AU (Sekanina & Kracht 2018). The nucleus appears to have survived the first outburst with only minor damage, releasing — as later determined (see below) — a companion undetected in a condensation of simultaneously dust ejecta before the onset of the second outburst. In the course of this event the nucleus was completely shattered into a massive cloud of rapidly expanding dust cloud, which obliterated the ejecta from the first outburst over a period of two weeks. As the ground-based observations were about to terminate, the measured astrometric positions ceased to fit the debris

¹⁰ See NASA website https://apod.nasa.gov/apod/image/0009/c99S4linear_000821-gg1.jpg.

from the second outburst and, instead, turned out to be consistent with the location of the companion released in the first outburst, implying its radial nongravitational acceleration of $16.9 \times 10^{-8} \text{AU day}^{-2}$, about 70 percent of ‘Oumuamua’s acceleration. In the absence of activity, this is an effect of solar radiation pressure, suggesting that the companion had a very high surface-area-to-mass ratio and represented an extremely fluffy aggregate of loosely-bound dust grains, a conclusion supported by the result derived directly from a nongravitational orbital solution linking all astrometric observations made prior to the second outburst.

These four examples show that for different perishing comets the process of disintegration does not pass through identical stages. None of them can serve as an analog for the parent comet of ‘Oumuamua, a dwarf object with the absolute magnitude ≥ 18 , because they all were much too bright (and massive), as documented in Table 2. Nonetheless, the apparent fragment of C/2017 S3 released during the first outburst and astrometrically measured for several days about one month later appears to be an object whose role in the disintegration process may have been a little like that of ‘Oumuamua, even though information on it is extremely limited. The data on C/1999 S4 suggest that fragments get rapidly depleted of ice; whether they survived as large boulders or were crumbled into pebbles and/or dust is unclear.

There are some dwarfs in Table 4 among the long-period comets in non-Oort Cloud orbits, but these are of course irrelevant. No useful information comes from cursory inspection of Table 5 containing a few dwarf objects in poorly known orbits, all of perihelion distance larger than is of interest, and appearing, with the exception of C/2013 K1, preperihelion.

9. CONSTRAINTS ON SHAPE, DIMENSIONS, AND MASS OF ‘OUMUAMUA

I submit that the Spitzer Space Telescope’s failure to detect ‘Oumuamua (Trilling et al. 2018) provides **strong evidence for preferring pancake over cigar shape**. This argument is supported by simply comparing the two models. Let the maximum projected area derived from the peak absolute brightness during the tumbling be X_{max} . Let the light curve’s amplitude be $2.5 \log \gamma$, where $\gamma > 1$ is the ratio of the maximum-to-minimum projected area. The long and short diameters of ‘Oumuamua in the case of cigar shape equal, respectively,

$$\begin{aligned} (D_{\text{max}})_{\text{cig}} &= \sqrt{\frac{4\gamma}{\pi} X_{\text{max}}} \\ (D_{\text{min}})_{\text{cig}} &= \sqrt{\frac{4}{\gamma\pi} X_{\text{max}}} = \frac{(D_{\text{max}})_{\text{cig}}}{\gamma}. \end{aligned} \quad (15)$$

The maximum and minimum diameters in the case of pancake shape amount to

$$\begin{aligned} (D_{\text{max}})_{\text{pan}} &= \sqrt{\frac{4}{\pi} X_{\text{max}}} \\ (D_{\text{min}})_{\text{pan}} &= \frac{1}{\gamma} \sqrt{\frac{4}{\pi} X_{\text{max}}} = \frac{(D_{\text{max}})_{\text{pan}}}{\gamma}. \end{aligned} \quad (16)$$

To determine X_{max} I adopt a peak R absolute magnitude of 21.7 by Drahus et al. (2018), more conserva-

tive than Jewitt et al. (2017) value, which is 0.2 mag brighter. Since Trilling et al. (2018) present their results as a function of a visual albedo, I converted the R magnitude to V with Jewitt et al.’s color index $V - R = +0.45$; this gives $X_{\text{max}} = 0.002/p_V \text{ km}^2$, where p_V is the visual geometric albedo. Trilling et al. provide upper limits of the dimensions for three different albedos, varying of course as $p_V^{-1/2}$ and being equivalent. Selecting $p_V = 0.1$, one of the three options, I determine $X_{\text{max}} = 0.02 \text{ km}^2$, compared to Jewitt et al.’s (2017) 0.025 km^2 . I accept Trilling et al.’s γ value of 6 to make the comparison fully compatible. Equations (15) and (16) result in $(D_{\text{max}})_{\text{cig}} = 391 \text{ m}$ and $(D_{\text{min}})_{\text{cig}} = 65 \text{ m}$ for cigar shape, but $(D_{\text{max}})_{\text{pan}} = 160 \text{ m}$ and $(D_{\text{min}})_{\text{pan}} = 27 \text{ m}$ for pancake shape. **Trilling et al.’s 3σ upper limits** are 341 m for the maximum diameter and 57 m for the minimum diameter, thus being **compatible only with the pancake-like model**.

The cigar-like and pancake-like configurations differ from one another in the object’s volume, Y , as well. Approximations by the prolate and oblate spheroids give, respectively,

$$\begin{aligned} Y_{\text{cig}} &= \frac{\pi (D_{\text{max}})_{\text{cig}}^3}{6 \gamma^2} = \frac{4}{3\sqrt{\gamma\pi}} X_{\text{max}}^{\frac{3}{2}} \\ Y_{\text{pan}} &= \frac{\pi (D_{\text{max}})_{\text{pan}}^3}{6 \gamma} = \frac{4}{3\gamma\sqrt{\pi}} X_{\text{max}}^{\frac{3}{2}}, \end{aligned} \quad (17)$$

showing that the volume of the pancake-like model is $\sqrt{\gamma}$ times smaller. A pancake-like configuration is also preferred because of perceived better dynamical stability for an extremely fluffy object.

Looking at the issue from the standpoint of the hypothesis that ‘Oumuamua is a *highly irregularly shaped fragment* of an interstellar comet, Equations (15) through (17) indicate that the **pancake-like model is a positively better approximation** to the object’s actual shape than the cigar-like model.

The next point is the problem of extremely high porosity needed for ‘Oumuamua as an aggregate of submicron-sized grains of dust to succeed. I address two basic constraints that concern the object’s mass: (i) it should satisfy the projected-area-to-mass ratio required by the detected nongravitational acceleration in its orbital motion and (ii) it should *by orders of magnitude* exceed the absolute lower limit implied by a cloud of unbound submicron-sized grains of equal projected area.

The ratio of the geometric projected area X to the mass \mathcal{M} of an object subjected to solar radiation pressure is given by

$$\frac{Q_{\text{pr}} X}{\mathcal{M}} = \frac{4\pi c G M_{\odot}}{\mathcal{L}_{\odot}} \beta, \quad (18)$$

where c is the speed of light, G is the universal gravitational constant, M_{\odot} and \mathcal{L}_{\odot} are the mass and luminosity of the Sun, and β is a dimensionless, heliocentric-distance independent quantity that measures an acceleration ratio of solar radiation pressure to solar gravitational attraction. Because of the scattering properties of dust grains, their cross sectional area for radiation pressure differs generally from their geometric cross sectional area. To account for this difference, Equation (18) contains a dimensionless quantity Q_{pr} , the efficiency factor for ra-

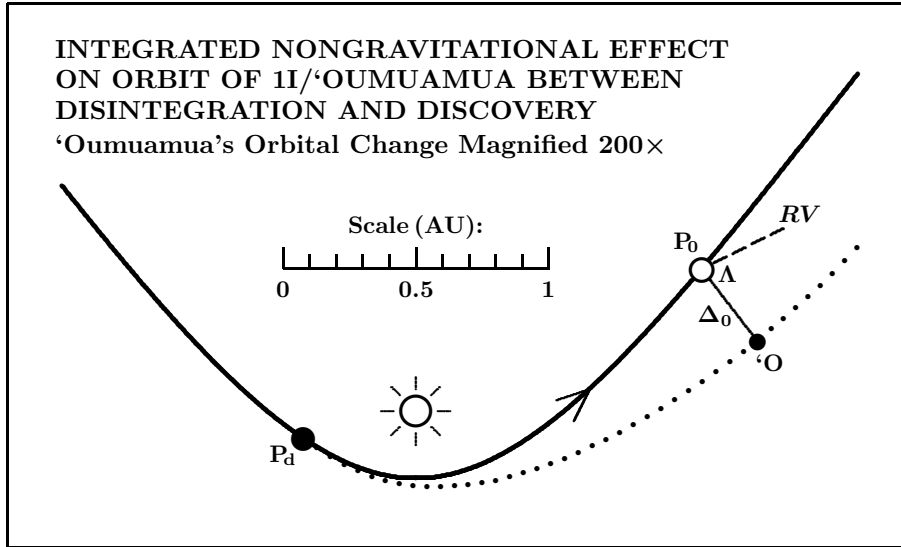


Figure 5. Integration of the orbital changes triggered by the nongravitational acceleration of 1I/‘Oumuamua between the time of disintegration of the parent comet and the time of ‘Oumuamua’s discovery. The solid curve is the orbit of the parent comet up to the point of its disintegration, P_d , assumed here to have occurred 10 days before perihelion. Within a fraction of its width, the solid curve is the orbit of ‘Oumuamua from the point P_d on. The arrow indicates the direction of orbital motion. The dotted curve is the orbit of ‘Oumuamua after the integrated effect of its nongravitational acceleration was magnified by a factor of 200. At the time of ‘Oumuamua’s discovery, the extrapolated position of the parent is marked by P_0 , the prolonged radius vector, shown as a dashed line, by RV . After magnification of the orbital changes of ‘Oumuamua, its position at the time of discovery is marked as ‘O, its distance from P_0 as Δ_0 , and the lag angle of its position vector behind the radius vector as Λ .

diation pressure that converts the latter to the former, but is generally close to unity.¹¹ With the standard values of the object independent quantities and $\beta = 0.00083$ for ‘Oumuamua, one has $\mathcal{M} = 0.092Q_{pr}X$, where X is in cm^2 and \mathcal{M} in g. Since the projected area varies quasi-periodically with time while the nongravitational acceleration is expressed as an averaged effect, it is likewise necessary to average the projected area exposed to sunlight. The method of averaging, which shows the result to depend on the axial ratio, is described in Appendix B; here I note that for the range of observed axial ratios the average projected area is 0.52 the peak area of 0.02 km^2 . Taking $Q_{pr} \simeq 1$ and rounding the result off, the predicted mass of ‘Oumuamua comes out to be

$$\mathcal{M} \simeq 1 \times 10^7 \text{ g}, \quad (19)$$

identical to the mass estimated by Sekanina & Kracht (2018). With the above dimensions this mass indicates that ‘Oumuamua’s bulk density is $\sim 0.00003 \text{ g cm}^{-3}$.

Although only loosely interconnected, submicron-sized particles in an aggregate should attenuate most incident sunlight, which requires that Oumuamua be orders of magnitude more massive than an optically thin cloud of submicron-sized grains of *equal* projected area. Compliance with this categorical condition is tested by comparing the mass of such a dust cloud with the above mass estimate of the object. Assuming that the aggregate consists of spherical grains $0.2 \mu\text{m}$ in diameter, the projected area of a single grain is $X_{gr} = \pi \times 10^{-10} \text{ cm}^2$. The number of grains needed to equal the peak projected area of ‘Oumuamua is $0.02 \text{ km}^2 / X_{gr} = 6.4 \times 10^{17}$. At an expected density of 3 g cm^{-3} , their total mass is 8000 g,

more than a factor of 10^3 lower than ‘Oumuamua’s estimated mass. On the average, only 0.08 percent of the projected surface of submicron-sized grains in the fluffy aggregate is exposed to sunlight, a very small fraction.

10. INTEGRATED ORBITAL CHANGES TRIGGERED BY ‘OUMUAMUA’S NONGRAVITATIONAL ACCELERATION

In the framework of the investigation of ‘Oumuamua as an interstellar comet’s fragment subjected to a nongravitational acceleration, one issue of particular interest is the orbital effect integrated over a period of time from the parent’s disintegration to ‘Oumuamua’s discovery. An example is displayed in Figure 5 for the parent’s disintegration time of 10 days before perihelion. The effect of an integrated nongravitational acceleration is magnified by a factor of 200 for clarity. The solid curve is the orbit of the parent up to the point P_d and of ‘Oumuamua from that point on (which coincides within the width of the drawn curve with the parent’s extrapolated orbit), while the dotted curve is ‘Oumuamua’s orbit after the application of the magnification factor. As seen, ‘Oumuamua moved in a slightly larger orbit and was at the time of discovery lagging a little behind the position it would occupy if there were no extra acceleration. The radial nongravitational acceleration of 0.000830 ± 0.000027 the Sun’s gravitational acceleration, which was derived by Micheli et al. (2018), has on ‘Oumuamua the same effect as if it were orbiting in a gravitational field of the Sun whose mass was reduced to 0.999170 ± 0.000027 its actual mass. The often noted “velocity boost” that ‘Oumuamua allegedly received from the nongravitational acceleration is misleading. The object’s location in the orbit relative to the unperturbed motion is time dependent and a function of the point of separation from the parent.

¹¹ For effects of radiation pressure on fluffy porous dust aggregates see, e.g., Kimura & Mann (1999), Tazaki & Nomura (2014).

Table 9

Nongravitational Effect Integrated Over Period of Time from Parent’s Disintegration to ‘Oumuamua’s Discovery

Time of Parent’s Disintegration ^a (days)	At Time of ‘Oumuamua’s Discovery			
	Separation in Space		Projected Onto Sky	
	Distance (10 ⁶ km)	Lag Angle ^b	Angular Separation	Position Angle
−40	0.242	99°5	26′8	126°7
−30	0.244	95.4	26.9	126.6
−20	0.249	89.4	27.2	126.4
−10	0.257	78.6	26.7	126.1
−5	0.250	68.6	23.9	125.7
−2	0.223	59.6	19.2	125.3
0	0.189	52.4	14.5	124.9
+2	0.147	45.0	9.7	124.4
+5	0.091	34.9	4.5	123.3
+10	0.041	23.0	1.2	120.2

Notes.

^a Reckoned from perihelion time; negative = before perihelion, positive = after perihelion.

^b Reckoned from prolonged radius vector clockwise toward orbit behind comet.

Since the disintegration time of the parent comet is not known, I assume for it a number of times between 40 days before perihelion and 10 days after perihelion. ‘Oumuamua is presumed to have acquired no separation velocity; the integrated effect is presented in Table 9 both as (1) its separation distance from the unperturbed position of the parent in the orbital plane and the lag angle reckoned from the prolonged radius vector toward the orbit behind the parent, as shown in Figure 5; and (2) an angular separation distance and the position angle in projection onto the plane of the sky.

Table 9 illustrates the enormity of the effect of the non-gravitational acceleration accumulated over only several weeks, with the separation distance growing to an astonishing quarter of a million kilometers with a large lag angle. This effect is of the same nature as the well-known striking post-perihelion broadening of dust tails of comets with small perihelion distance, a consequence of the law of conservation of orbital angular momentum. In practical terms it means that individual pieces of the debris that the parent’s disintegration resulted in were by the time of ‘Oumuamua’s discovery scattered over a huge volume of space, with a negligibly low spatial density. As obviously the largest of these fragments (subjected to the lowest acceleration), ‘Oumuamua was the only one detected. In terms of the angular separation in the sky, the effect amounts to nearly one half degree. Again, other fragments, if there are any, could easily be scattered over many degrees from the unperturbed position and would be missed except perhaps by large wide-field instruments. The peculiar lack of variation in the position angle is caused by the Earth being located only 1°.7 below the orbital plane as viewed from ‘Oumuamua.

11. FINAL COMMENTS AND CONCLUSIONS

The post-perihelion discovery of ‘Oumuamua has left open the question of its relationship to the interstellar object that had entered the inner regions of the Solar

System: Was ‘Oumuamua identical to this object or did the object experience shortly before or at perihelion a disintegration event whose product ‘Oumuamua has become — a large piece of debris of the parent? The answer is of course a matter of conjecture that depends on the starting postulates on which the argument is formulated. The fundamental postulate of this study is that the **object was an active interstellar comet** whose morphology and related physical properties were **similar** to those of the **Oort Cloud comets**, a plausible hypothesis given that both were exposed to the same kind of environment over an extended period of time. In addition, in order to comply with the nondetection in the PanSTARRS’s June 2017 images, the comet’s activity should have been very low. The object is therefore classified as a **dwarf comet**, with the synoptic index exceeding +16. Under these conditions it is absolutely impossible to escape the conclusion that **‘Oumuamua’s parent inevitably perished near perihelion**, most probably shortly before perihelion, and that **‘Oumuamua is a major fragment of the original comet**, possibly the only surviving piece of debris of substantial mass.

‘Oumuamua is often described as unlike any other cosmic object ever detected. The present results question whether any known Oort Cloud comet is intrinsically as faint or fainter. The absolute magnitude of the faintest one among those listed in this paper, C/2005 K2, is 13.5 (Tables 1, 2, and 6), compared to an estimated absolute magnitude of ≥ 18 for ‘Oumuamua (Sekanina 2019). For this reason, evidence on the debris of the best examined perishing Oort Cloud comets (Section 8) is not quite relevant to ‘Oumuamua or its parent comet, except for obvious features, such as the absence of outgassing by an ice depleted fragment. The strongest evidence dictating the extremely low bulk density and super fluffy nature of ‘Oumuamua (Sekanina 2019) is of course the **detected nongravitational acceleration** (Micheli et al. 2018), which could hardly be **driven by** anything else than **solar radiation pressure**, given the nonexistence of activity. As noted in Section 8, a similar kind of object appears to have been briefly detected in C/2017 S3, but only little relevant information is available.

The enormous amplitude of ‘Oumuamua’s light curve is overwhelmingly interpreted as shape driven, although a contribution from albedo variations over the surface is sometimes invoked (e.g., Jewitt et al. 2017). The clear preference for cigar shape over pancake shape in the literature may be influenced by the fact that the several nuclei (of the short-period comets) of known figure resemble a prolate rather than oblate spheroid. However, the critical **nondetection of ‘Oumuamua by the Spitzer Space Telescope implies compatibility with optical data for pancake shape but not for cigar shape**.

The extremely high porosity is perhaps unique for a comet-like object, but the estimated mass of ‘Oumuamua is still more than three orders of magnitude higher than the mass of a cloud of unbound submicron-sized particles of the same total projected area. Accordingly, the implied fluffy structure does significantly attenuate sunlight not only because of the low albedo. It is expected that ‘Oumuamua’s dimensions do not exceed the ones determined from optical observations.

The magnitude of the nongavitational acceleration, equivalent to 83×10^{-5} the solar gravitational attraction

is by no means minuscule. Its integrated effect over the period of time between the parent comet’s presumed disintegration and ‘Oumuamua’s discovery equals, depending on the former’s time, up to more than 250 000 km and nearly 0.5° in projection onto the plane of the sky. Whereas the spatial separation was of course increasing with time, the projected separation was decreasing because of ‘Oumuamua’s rapidly increasing distance from the Earth. A lesson learned from this exercise is that **any potential lesser fragments should have been scattered over a large area of the sky** at the discovery time, when they were at their brightest for terrestrial observers.

The breakup event of the parent comet near perihelion has, besides the potentially overwhelming effect on ‘Oumuamua’s morphology, other implications. One concerns the question of the delicate fluffy structure’s survival over a long period of time. If this property were intrinsic to the object before its arrival to the Solar System, one would have to demonstrate that it was able to survive interstellar travel. In the hypothesis proposed in this paper, the structure’s lifetime on the order of 200 days would safely warrant its survival over a period ending with the object’s last observation; in fact, moderate instability and/or fragmentation may not have been observationally recognized during this time span. The other implication is the impact on investigations aimed at establishing the stellar system from which ‘Oumuamua had arrived. Given that the time of the disintegration event is unknown and that, in addition, the orbital motion of the parent comet may have been affected by an outgassing-driven nongravitational acceleration of unknown magnitude, the velocity determination of the parent’s initial incoming velocity in interstellar space is unfortunately compromised.

We never have had a chance to inspect — and may not have in the foreseeable future — a closeup image of the nucleus of an Oort Cloud comet, and details of its nature remain unknown. Comparison with other long-period comets near the Sun suggests that **Oort Cloud comets are very different, showing the strong propensity for disintegrating near perihelion, especially when close to the Sun.** Their nuclei appear to **experience major problems in tolerating the environment of relentless solar heating**, ever more so as heliocentric distance decreases. These difficulties are **most obvious among the intrinsically faint objects** (presumably low in mass) and **the objects depleted in dust.** In fact, the only two Oort Cloud comets between 2000 and 2017 observed to have survived in orbits with perihelion distance not exceeding 0.3 AU, C/2006 P1 and C/2011 L4, were both very bright (and presumably massive) and dust-rich objects. It is proposed that massive comets have a greater chance to survive because of their substantial reservoirs of ice, whose sublimation is instrumental in keeping the surface temperature under control; and that dust-rich comets are able to better protect the surface of the nucleus by saturating the atmosphere with microscopic dust to the point of making it optically thick while close to the Sun.

By contrast, nearly all **other long-period comets** investigated in this paper **survive perihelion**, perhaps because of the presence of a protective mantle of sintered dust on the surface of their nuclei. The process of sudden disappearance is among these (as well as short-period) comets restricted to short-lived companions of the split

comets (see Section 10 of Sekanina & Kracht 2018) and to other isolated cases (e.g., 3D/Biela, 5D/Brorsen, 20D/Westphal), all of which are independent of the heliocentric distance at perihelion. These topics are outside the scope of this paper. So is the problem of disappearance of the dwarf sungrazers of the Kreutz system, which sublimate away under extremely high temperatures.

The perihelion survival limit for long-period comets, proposed by Bortle (1991) as the minimum absolute brightness that the comet has to have in order to survive, turned out to be too low: about one third of the Oort Cloud comets investigated in this study — in both the 2000–2017 and 1989–1999 sets — that were predicted by this rule to survive did in fact perish. In an effort to remedy this problem, I propose a **synoptic index $\mathfrak{S}_{\text{surv}}$ as a new perihelion survival predictor**, but this issue should by no means be considered closed. A larger and more accurate data base should in the future allow a better understanding of the nucleus’ properties of Oort Cloud comets in general and the forces that determine their surviving or perishing near the Sun in particular.

One comet, C/2016 U1, appears to have survived, defying both Bortle’s rule and the $\mathfrak{S}_{\text{surv}}$ index. I question whether this comet was at all an Oort Cloud comet rather than an interloper that was masquerading as a member thanks to the planetary perturbations that in the previous return to the Sun modified its orbit by increasing its aphelion toward the Oort Cloud; in fact, this comet’s Oort Cloud membership is already open to doubt on account of the fairly large uncertainty of its computed original semimajor axis.

In closing, I remark that the proposed morphological similarity of ‘Oumuamua and its parent comet with the Oort Cloud comets opens up intriguing possibilities for research of interstellar objects. The investigation of perihelion survival of the Oort Cloud comets provides a remarkable insight into the nature of their nuclei, especially in the absence of their closeup imaging. It is hoped that this paper will stimulate increased interest in these and the other examined issues.

This research was carried out at the Jet Propulsion Laboratory, California Institute of Technology, under contract with the National Aeronautics and Space Administration.

APPENDIX A

ACCOMMODATION LIMIT, SYNOPTIC INDEX, AND EQUIVALENT PERIHELION DISTANCE FOR STRONGLY HYPERBOLIC ORBITS

As the expression for the rate of increase in the solar flux, $\dot{\mathcal{F}}_{\odot}$, depends in part on the object’s orbital velocity, Equation (6) applies strictly only to parabolic motion, with high accuracy also to Oort Cloud comets. It does not apply to objects in strongly hyperbolic orbits, such as 1I/‘Oumuamua or its parent comet. Because of the higher orbital velocity, the rate of increase in the solar flux at a heliocentric distance r along a hyperbolic orbit, $(\dot{\mathcal{F}}_{\odot})_{\text{h}}(r; q, e)$, *exceeds* the rate along a parabolic orbit of equal perihelion distance, $(\dot{\mathcal{F}}_{\odot})_{\text{p}}(r; q)$. The same applies to the peak rates. To account for this difference in the

expression for the accommodation limit \mathcal{A} and in a plot of H_0 against q , as well as in the formula for the synoptic index $\mathfrak{S}_{\text{surv}}$, one should replace the perihelion distance q of the hyperbolic orbit with a perihelion distance q' of an equivalent parabolic orbit ($q' < q$), so that the peak rates of increase in the solar flux match each other,

$$(\dot{\mathcal{F}}_{\odot})_{\text{h,max}}(q, e) = (\dot{\mathcal{F}}_{\odot})_{\text{p,max}}(q'). \quad (20)$$

The general expression for the radial velocity is

$$\dot{r} = \frac{ke \sin u}{\sqrt{q(e+1)}}, \quad (21)$$

where k is the Gaussian gravitational constant and u is the true anomaly ($u < 0$ before perihelion). Providing u in terms of heliocentric distance, the expression for the rate of increase in the solar flux along a hyperbolic orbit has a form

$$(\dot{\mathcal{F}}_{\odot})_{\text{h}}(r; q, e) = 2k \frac{\mathcal{F}_0}{r^3} \sqrt{\frac{e-1}{q}} \left[1 + \frac{q}{r} \frac{2}{e-1} - \left(\frac{q}{r}\right)^2 \frac{e+1}{e-1} \right]^{\frac{1}{2}}. \quad (22)$$

The rate of increase in the solar flux along a hyperbolic orbit reaches a peak of

$$(\dot{\mathcal{F}}_{\odot})_{\text{h,max}}(q, e) = k\mathcal{F}_0 q^{-\frac{7}{2}} f^{-\frac{7}{2}} \sqrt{g} \quad (23)$$

at

$$r_{\text{h,max}}(q, e) = fq, \quad (24)$$

where

$$f = \frac{\sqrt{1 + 48e^2} - 7}{6(e-1)} \quad (25)$$

and

$$g = 8 \left(1 + \frac{e-1}{2} f - \frac{e+1}{2f} \right). \quad (26)$$

According to Equation (20), the perihelion distance of the equivalent parabolic orbit, q' , is determined by equating the expressions (4) at q' and (23) at q . The result is

$$q' = \frac{7f}{8} g^{-\frac{1}{7}} q. \quad (27)$$

First, in the limiting parabolic case, one has $e \rightarrow 1$ and by L'Hospital's Rule $f \rightarrow \frac{8}{7}$, which implies $g \rightarrow 1$ and, from Equation (27), $q' \rightarrow q$, as expected. Since 'Oumuamua's elements are $q = 0.255$ AU, $e = 1.20$, one finds for its *equivalent* perihelion distance $q' = 0.973q = 0.248$ AU, thereby correcting q for the effect of the hyperbolic excess. The deviation from the nominal perihelion distance is trivial — less than 3 percent — and can safely be neglected in the first approximation.

APPENDIX B

AVERAGING PROJECTED AREA OF SUNLIT FRACTION OF OBLATE SPHEROID'S SURFACE OVER ALL DIRECTIONS

In compliance with the conclusions of Section 9 I assume that 'Oumuamua's figure is approximated by an oblate spheroid, whose semiaxes are a , a , and b ($b < a$) and whose maximum projected area in the equatorial plane equals πa^2 . Let $\gamma = a/b$ and the Sun make an

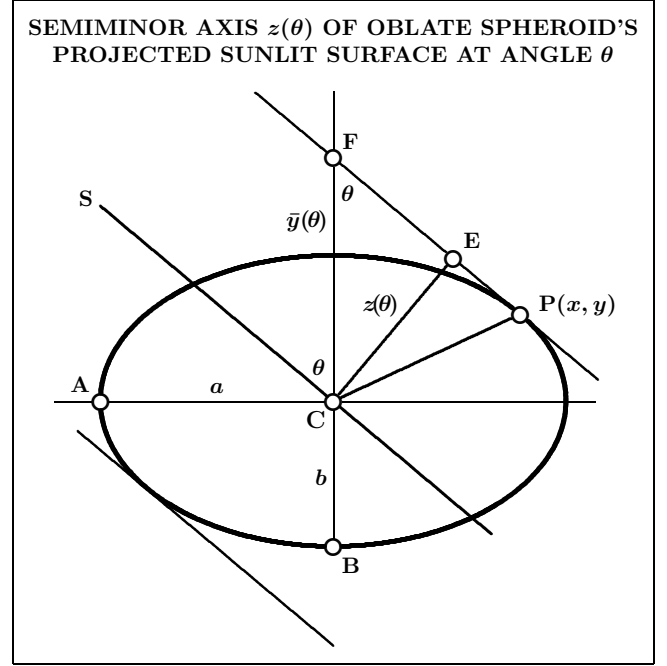


Figure B.1. Determination of the semiminor axis $z(\theta)$ of an oblate spheroid's projected sunlit surface at an angle θ . The spheroid, centered at C and of semimajor axis $a = AC$ and semiminor axis $b = BC$, is viewed from a point in its equatorial plane in a direction perpendicular to incoming sunlight along the line SC . The tangent FP to the spheroid, parallel to SC , delimits the ordinate $\bar{y} = CF$ and the semiminor axis $z(\theta) = CE$ of the sunlit area, whose projected area is $\pi a z(\theta)$.

angle of θ with the normal to the equatorial plane, as shown in Figure B.1. The other angle, ϕ , is reckoned along the equatorial plane. The task is to determine the projected area of the fraction of the spheroid's surface that is sunlit (and therefore subjected to solar radiation pressure) when averaged over all directions. From Figure B.1 it follows that at an angle θ the projected sunlit area is an ellipse whose semimajor axis is a , semiminor axis is $z(\theta)$, and the cross section perpendicular to SC is $\pi a z(\theta)$. Here $z(\theta) = CE$ and point E lies on a tangent to the spheroid that passes through point $P(x, y)$ and is parallel to the direction SC . The tangent intersects the normal to the equatorial plane at point F, delimiting an ordinate \bar{y} and making angle θ with the normal.

To determine the length of $z(\theta)$, I begin with an equation of the spheroid in projection onto a plane perpendicular to the equatorial plane, with the origin $C(x_0, y_0)$ at $x_0 = 0, y_0 = 0$,

$$\frac{x^2}{a^2} + \frac{y^2}{b^2} = 1. \quad (28)$$

Introducing $\gamma = a/b$ ($\gamma > 1$), one has for the tangent to the ellipse at point $P(x, y)$

$$\frac{dy}{dx} = -\frac{x}{\gamma^2 y} = \tan(90^\circ + \theta) = -\cot \theta, \quad (29)$$

so that

$$x = \gamma^2 y \cot \theta. \quad (30)$$

To separate x from y , I insert for x from Equation (30)

Table B.1
Sunlit Fraction of Oblate Spheroid's Surface
Averaged Over All Directions As Function
of Ratio γ of Major to Minor Axis

Axial Ratio γ	Spheroid's Oblate- ness	Light Curve Amplitude (mag)	Averaged Sunlit Surface Fraction
1	0.000	0.00	1.000
1.2	0.167	0.20	0.891
1.5	0.333	0.44	0.787
2	0.500	0.75	0.690
2.5	0.600	1.00	0.637
3	0.667	1.19	0.604
4	0.750	1.51	0.567
5	0.800	1.75	0.547
7	0.857	2.11	0.527
10	0.900	2.50	0.515
15	0.933	2.94	0.508
∞	1.000	∞	0.500

Note.

First entry refers to a sphere, last to a flat circular disk.

into Equation (28), which gives

$$y = \frac{a \sin \theta}{\gamma \sqrt{1 + (\gamma^2 - 1) \cos^2 \theta}}, \quad (31)$$

and back from (30),

$$x = \frac{a\gamma \cos \theta}{\sqrt{1 + (\gamma^2 - 1) \cos^2 \theta}}. \quad (32)$$

The ordinate \bar{y} is computed from

$$\bar{y} = y + x \cot \theta, \quad (33)$$

allowing one to find for $z(\theta)$ an expression,

$$z(\theta) = \bar{y} \sin \theta = \frac{a}{\gamma} \sqrt{1 + (\gamma^2 - 1) \cos^2 \theta}. \quad (34)$$

The projected area of the sunlit fraction of the spheroid's surface, averaged over the hemisphere, $\langle X \rangle$, is now derived by integrating over all angles θ from 0 to $\frac{1}{2}\pi$ and over all angles ϕ [which $z(\theta)$ is independent of] from 0 to 2π :

$$\int_0^{2\pi} d\phi \int_0^{\frac{\pi}{2}} \langle X \rangle \sin \theta d\theta = \int_0^{2\pi} d\phi \int_0^{\frac{\pi}{2}} \pi a z(\theta) \sin \theta d\theta \quad (35)$$

with $z(\theta)$ from Equation (34). Employing a substitution $\psi = \cos \theta$, Equation (35) becomes to

$$\begin{aligned} \langle X \rangle &= \frac{\pi a^2}{\gamma} \int_0^1 \sqrt{1 + (\gamma^2 - 1)\psi^2} d\psi \\ &= \frac{\pi a^2}{2} \left[1 + \frac{\ln(\gamma + \sqrt{\gamma^2 - 1})}{\gamma \sqrt{\gamma^2 - 1}} \right], \end{aligned} \quad (36)$$

which is the resulting relation. Since πa^2 is the maximum projected area of the spheroid, this formula indicates that the averaged projected area $\langle X \rangle$ is never smaller than $\frac{1}{2}$ the maximum. It is equal to this value when $\gamma \rightarrow \infty$, i.e., for a flat circular disk. At the other extreme, $\langle X \rangle$ equals πa^2 when $\gamma = 1$, i.e., for a sphere, as expected. The

averaged projected area of all spheroids ($1 < \gamma < \infty$) is larger than one half of, and less than, the maximum area.

The variation of the averaged sunlit surface fraction, $\langle X \rangle / \pi a^2$, with the ratio γ is listed in Table B.1; also included are the oblateness, $(\gamma - 1)/\gamma$, of the spheroid and the amplitude of the light curve. For $6 \leq \gamma \leq 11$, the range of axial ratios relevant to the light curve of 'Oumuamua, the averaged sunlit surface fraction is restricted to 0.52 ± 0.01 .

REFERENCES

- A'Hearn, M. F., Schleicher, D. G., Millis, R. L., et al. 1984, *AJ*, 89, 579
A'Hearn, M. F., Millis, R. L., & Schleicher, D. G. 1995, *Icarus*, 118, 223
Bonev, T., Jockers, K., Petrova, E., et al. 2002, *Icarus*, 160, 419
Borisov, G., Bonev, T., Iljev, I., & Stateva, I. 2012, *Bulg. Astron. J.*, 18, 47
Bortle, J. E. 1991, *Int. Comet Quart.*, 13, 89
Camilleri, P. 1994, *IAUC* 5995
Curdtt, W., Boehnhardt, H., & Vincent, J.-B. 2014, *A&A*, 567, L1
Drahus, M., Guzik, P., Waniak, W., et al. 2018, *Nature Astron.*, 2, 407
Farnham, T. L., Schleicher, D. G., Woodney, L. M., et al. 2001, *Science*, 292, 1348
Ferrín, I. 2014, *MNRAS*, 442, 1731
Fink, U., & Rubin, M. 2012, *Icarus*, 221, 721
Gehrz, R. D. 1992, *IAUC* 5482
Gilmore, A. C. 1994, *IAUC* 6004
Green, D. W. E. 2004, *IAUC* 8346
Green, D. W. E. 2005, *IAUC* 8540
Guido, E., Sostero, G., & Howes, N. 2011, *CBET* 2876
Hale, A. 1992, *IAUC* 5496
James, N. 2017, *JBAA*, 127, 132
Jehin, E., Boehnhardt, H., Sekanina, Z., et al. 2002, *Earth Moon Plan.*, 90, 147
Jewitt, D., Luu, J., Rajagopal, J., et al. 2017, *ApJ*, 850, L36
Jorda, L., Hainaut, O., & Smette, A. 1995, *Plan. Space Sci.*, 43, 737
Keane, J. V., Milam, S. N., Coulson, I. M., et al. 2016, *ApJ*, 831, 207
Kidger, M. R. 2002, *Earth Moon Plan.*, 90, 157
Kidger, M. R., Altieri, B., Müller, T., & Gracia, J. 2016, *Earth Moon Plan.*, 117, 101
Kimura, H., & Mann, I. 1998, *J. Quant. Spec. Rad. Transf.*, 60, 425
Knight, M. M., & Battams, K. 2014, *ApJ*, 782, L37
Kobayashi, T. 1992, *IAUC* 5496
Korsun, P., Kulyk, I., & Velichko, S. 2012, *Plan. Space Sci.*, 60, 255
Kronk, G. W. 2003, *Cometography: A Catalog of Comets, Volume 2: 1800–1899* (Cambridge, UK: Cambridge University Press), 900pp
Li, J., & Jewitt, D. 2015, *AJ*, 149, 133
Machholz, D. E. 1994, *J. Assoc. Lunar Plan. Obs.*, 37, 171
Machholz, D. E. 1996, *J. Assoc. Lunar Plan. Obs.*, 39, 71
Mäkinen, J. T. T., Bertaux, J.-L., Combi, M. R., & Quémerais, E. 2001, *Science*, 292, 1326
Marcus, J. N. 2007, *Int. Comet Q.*, 29, 39
Marsden, B. G. 1990, *AJ*, 99, 1971
Marsden, B. G. 2000a, *MPEC* 2000-O07
Marsden, B. G. 2000b, *MPC* 28557
Marsden, B. G., & Williams, G. V. 2008, *Catalogue of Cometary Orbits* 2008, 17th ed. (Cambridge, MA: IAU Minor Planet Center/Central Bureau for Astronomical Telegrams), 195pp
Marsden, B. G., Sekanina, Z., & Yeomans, D. K. 1973, *AJ*, 78, 211
Marsden, B. G., Sekanina, Z., & Everhart, E. 1978, *AJ*, 83, 64
Mattiazzo, M. 2003, *IAUC* 8250
Mattiazzo, M., & McNaught, R. H. 2011, *CBET* 2801
Micheli, M., Farnocchia, D., Meech, K. J., et al. 2018, *Nature*, 559, 223
Moreno, F., Pozuelos, F., Aceituno, F., et al. 2014, *ApJ*, 791, 118
Nakano, S. 1996, *MPC* 28557
Opitom, C., Jehin, E., Manfroid, J., & Gillon, M. 2013, *CBET* 3433
Osip, D., Schleicher, D., & Campins, H. 1993, *Lunar Plan. Inst., Contr.* 810, 241
Protospapa, S., Kelley, M. S. P., Yang, B., et al. 2018, *ApJ*, 862, L16
Rosenbush, V. K., Velichko, F. P., Kiselev, N. N., et al. 2006, *Solar Syst. Res.*, 40, 290
Schleicher, D. G., & Osip, D. J. 1990, *IAUC* 4983
Scotti, J. V. 1994, *IAUC* 6004
Sekanina, Z. 1984, *Icarus*, 58, 81

- Sekanina, Z. 2002, *Int. Comet Quart.*, 24, 223
Sekanina, Z. 2005, *IAUC* 8545
Sekanina, Z. 2011, *CBET* 2876
Sekanina, Z. 2019, eprint arXiv:1901.08704
Sekanina, Z., & Kracht, R. 2014, eprint arXiv:1404.5968
Sekanina, Z., & Kracht, R. 2016, *ApJ*, 823, 2
Sekanina, Z., & Kracht, R. 2018, eprint arXiv:1812.07054
Sekanina, Z., Jehin, E., Boehnhardt, H., et al. 2002, *ApJ*, 572, 679
Seki, T. 1992, *IAUC* 5496
Shanklin, J. D. 1997, *JBAA*, 107, 186
Shanklin, J. D. 1998, *JBAA*, 108, 305
Shanklin, J. D. 2001, *JBAA*, 111, 247
Shanklin, J. D. 2009, *JBAA*, 119, 317
Tazaki, R., & Nomura, H. 2015, *ApJ*, 799, 119
Tomita, K. 1962, *IAUC* 1787
Tozzi, G. P., Boehnhardt, H., Hainaut, O. R., et al. 2003, *IAUC* 8250
Trilling, D. E., Mommert, M., Hora, J. L., et al. 2018, *AJ*, 156, 261
Vsekhsvyatsky, S. K. 1958, *Fizicheskie kharakteristiki komet.* (Moscow: Gosud. izd-vo fiz.-mat. lit.); translated: 1964, *Physical Characteristics of Comets*, NASA TT-F-80 (Jerusalem: Israel Program for Scientific Translations)
Weaver, H. A., Sekanina, Z., Toth, I., et al. 2001, *Science*, 292, 1249
Whipple, F. L. 1975, *Mém. Soc. Roy. Sci. Liège, Sér. 6*, 9, 101
Whipple, F. L. 1978, *Moon & Plan.*, 18, 343